Design and investigation of reflectivity based optofluidic devices

Seow Yong Chin

(B.ENG., Nanyang Technological University)

A THESIS SUBMITTED

FOR THE DEGREE OF DOCTOR OF PHILOSOPHY

DEPARTMENT OF MECHANICAL ENGINEERING

NATIONAL UNIVERSITY OF SINGAPORE

2013

DECLARATION

I hereby declare that this thesis is my original work and it has been written by me in its entirely. I have duly acknowledged all the sources of information which have been used in the thesis.

This thesis has also not been submitted for any degree in any university previously.

Seow Yong Chin

Date: 29th May 2013

ACKNOWLEDGEMENTS

I would like to express my deep gratitude towards my supervisors Associate Professor Lee Heow Pueh and Associate Professor Lim Siak Piang for supporting me in research to complete this thesis. Their guidance, supervision and guidance are crucial for the completion of the four years of research and study. With their support, I pushed myself hard to deliver research results.

I would also like to thank Dr. Wang Zhen Feng and all the technical staffs in the Applied Mechanics Laboratory for their assistance in various fabrication and technical matters. I wish to take this opportunity to convey my gratitude to National University of Singapore for providing me with Research Scholarship. I also like to thank Professor Khoo Boo Cheong, Professor Liu Ai Qun and Dr. Yang Yi for their sincere help and encouragement throughout this period of time.

My appreciation also goes to my family members: my parents Seow Woon Fah and Loh Swee Lan, my grandpa Seow Hoi You and grandma Siew Tai. Their dedication and support in my university education were critical. I also like to express deep gratitude towards friends that always be presence and consistently supports me mentally in this difficult and challenging period of my life.

Finally, I would like to thank Dr. Song Wu Zhou and Dr. Liang Yen Nan for their help in my studies. The lifelong friendship will be always remembered.

TABLE OF CONTENTS

SUMMARY

Optofluidic is the technology synthesis between optics and microfluidics that enables the development of various miniaturized optical systems. The optofluidic compartments provide seamless integration with micro-total analysis (μ-TAS) systems. Optofluidic technologies provide optical tunability which its solid counterparts lack. Furthermore, the creation of optofluidic technologies in planar microfluidic devices represents an importance aspect in the integration of optical functionalities into μ-TAS systems. All solid based optical systems, take for instance, those that are built by glass or semiconductor material cannot be integrated into the current state-of-the-art μ-TAS systems. The physical properties or the direction of light can be altered within the optofluidic circuit utilizing optical reflectivity's property at solid-liquid interfaces or liquid-liquid interfaces. These light manipulation technologies are able to cater for a broad range of applications.

Light switching is a fundamental light manipulation technique. However, there is no light switching functionality existing in optofluidic technologies. A novel hydrodynamic focusing microstructure is simulated in FEMLAB. The simulation results show the microstructure's capability to reconfigure the fluid-fluid interfaces. The microchannels are designed and fabricated on silicon wafer. The polydimethylsiloxane (PDMS) chip fabricated from the silicon mold is used for optical experiment to detect the power loss in the optical switching experiments. A 1 inlet 2 outlets optical switch is realized with optofluidic technology by utilizing the principle of total internal reflection (TIR), reconfigurable fluid-fluid interfaces and angle of light incidence greater than critical angle. The aforementioned optofluidic switch has many advantages over its solid counterparts. It has made a

step towards integration of optical switch within the planar PDMS chip, ready to be integrated with other functionalities based on microfluidic technologies. It has two drawbacks which need to be addressed. The limited amount of switching positions and the limited lifespan poses challenges when the optofluidic switch is incorporated. Consequently, solid-fluid interfaces are introduced to realize optical switching. The photonic chip used for optical experiment is found to achieve lifespan of approximately 220 times more than the traditional optofluidic compartments. This is the first report on solid-liquid interfaces used in planar optical switching, which realized one input three outlets optical switching.

When the light switches from one outlet to another, it undergoes partial refraction before TIR occurs. This transition is controlled by the change of refractive index of the fluid within the microchannel. On the contrary, the amount of the light refracted as the optical reflectivity of the solid-liquid interfaces changes can become a gauge to measure the refractive index inside the microchannel. With the same soft lithography process, the microchannels are fabricated onto the PDMS chip. The refractive index sensing experiment is conducted by observing the reflected light intensity for different optical reflectivity of the solid-liquid interfaces. Refractive index sensing resolution of 0.01 is achieved with the sensing technique based on partial refraction in planar PDMS devices. With the same optical principle of optical refraction, the fluid-solid optical surfaces are curved rather than flat, which is studied in the previous three chapters to investigate the light manipulation capabilities in chapter 5. Tunable optical diverging, collimating and focusing are realized by the optofluidic variable-focus lenses. This thesis has contributed towards the integration of optical partial refraction, tunable optical diverging, focusing, collimating, and switching within the planar optofluidic devices.

NOMENCLATURE

n_t	Refractive index of the transmittance medium
n_i	Refractive index of the incidence medium
θ_i	Incident angle
θ_t	Transmittance angle
R	Optical reflection constant
n_l	Refractive index of the fluid residing within the lens
n_p	Refractive index of the PDMS
R_l	Radius of curvature of the left solid-fluid optical interface of the lens cavity
R_r	Radius of curvature of the right solid-fluid optical interface of the lens cavity
f	Focal length of the lens
t	Thickness of the lens
s	Distance between the optical fiber and the central of the lens

LIST OF FIGURES

Chapter 1

Introduction

1.1.1 Microfluidic system for biomedical analysis

Microfluidic systems with reconfigurable optical systems have many unique properties that the non-configurable counterparts cannot achieve. Take for instance, microfluidic systems have the advantages of fluid and optical tunability. The microfluidic systems can shorten the time for analysis, lower production cost, reduce sample or reagent volume, and reduce power consumption. These advantages have contributed to considerable interest in a field known as microfluidic. This research field was initiated by the Defense Advanced Research Projects Agency (DARPA) of the US Department of Defense in the 1990s. It aims to develop field-deployable microfluidic systems. Microfluidic can manipulate small amount (10^{-9} to 10^{-18} liters) of sample or reagent within the microchannel. The conventional fabrication techniques for lab-on-a-chip applications rely on glass and silicon etching [1]. However, using these techniques, the devices are expensive and involve complex fabrication processes. These methods have inherent disadvantages in the creation of new lab-on-a-chip devices.

1.1.2 Optofluidic technology applied in microfluidic circuit

The traditional optical systems that are made of glass utilizes free space optical coupling. They cannot be miniaturized and incorporated into the polydimethylsoloxane (PDMS) based lab-on-a-chip applications. The integration of

optical systems fabricated by semiconductor material with PDMS based microfluidic chip is not feasible. Moreover, the optical systems fabricated using semiconductor materials have low visibility for its lightpath. The light output can only be detected by complicated and costly equipment. Due to the aforementioned disadvantages of the glass and silicon based devices, the current state-of-the-art optics components, for instance, lenses, switches, sensors, and waveguides cannot be seamlessly integrated within the lab-on-a-chip applications. The optical interfaces and the refractive indexes of the solid based optical systems are not tunable, unlike the optofluidic devices based on fluid-fluid interfaces.

A lot of research effort has been put into combining integrated micro-optical devices with microfluidic systems. This research field is termed as optofluidic. A new range of optofluidic compartments based on different optics principles aim to achieve optical excitation, sensing, and switching in optical detection systems. The absence of turbulence when the fluid flows in the scale of tens of micrometers is known as laminar flow. The physical characteristics of the fluid-fluid interfaces can be controlled via adjusting the flow rates on the micrometer or nanometer scale. When there is diffusion between the fluid-fluid interfaces, the fluid-fluid interfaces exhibit gradient refractive index profile. When the diffusion is absent at the fluid-fluid interfaces, it exhibits laminar flow's characteristic. Janasek et al. [2] described the scaling relations that related them to macroscopic and microfluidic systems. Using this phenomenon, many optofluidic devices have been created, for instance, filter [3], lenses [4], optical switch [5], and light source [6]. Optofluidic devices can cater for these purposes utilizing various optical principles such as surface-plasmon-resonance [7-8], Fabry-Perot interferometer [9], evanescent wave [10], interference [11], and long period grating [12].

The advancement of the optofluidic technology with the state-of-the-art lithography technology has realized many optical manipulation techniques on the micrometer or nanometer scale [1][3-8]. Optofluidic technology also enables the mass implementation of the optics compartments in current state-of-the-art optofluidic devices. In the recent development of microfluidic devices, optofluidic gradually becomes important optical compartments in lab-on-a-chip systems. The research on optofluidic compartments will create fundamental and technological advances in optical devices and sensor applications.

Lab-on-a-chip devices can be categorized into four broad areas: miniaturized analytical systems, biomedical devices, tools for chemistry and biochemistry, and systems for fundamental research. The ultimate goal is to integrate different optical components such as lenses, filters, and interferometers onto a single chip that encapsulates different capabilities for biochemistry or optical analysis. It is achieved by implementing novel microfluidic structures. These technologies can be combined with the knowledge of medical community to use microfluidic chips in diagnosing diseases while reducing the capital expense. The creations of these optofluidic compartments within the planar microfluidic circuits enable the seamless integrations of optical functionalities with other microfluidic functionalities for functional lab-on-a-chip applications. Take for instance, it allows the design for multi-sample analysis platforms in bio-medical devices involving micro-assay sensing. The micro-array sensing related to detecting biochemical phenomena and imaging tissue could benefit from the optofluidic devices integrated in the microchips.

1.1.3 Optofluidic technology for optical sensing and excitation

Optofluidic technologies [1][13] reduce the size of the microsystem for optical sensing and excitation to micrometer or nanometer scale. Consequently, the fluid analyte needed for sensing is reduced significantly. In some cases of refractive index sensing by optofluidic technology, fluorescence labeling is not needed. A label-free sensing technology is convenient and represents a major development compared to the traditional fluorescence based sensing technology. Refractive index sensing is crucial in the analysis of substances in many biochemical applications [14-15]. Similarly, the optofluidic refractive index sensor also inherits the aforementioned advantages of the label free sensing technology. The optofluidic technique can achieve efficient cost-performance ratio, as a single layer of lithography can simplify the rapid prototyping process. Designing the optofluidic compartments with microfluidic and optical tunability is important for optical sensing applications [1]. Optical excitation is also another important feature in lab-on-a-chip microsystem, enabling subsequent optical sensing applications like the fluorescent based sensing. Consequently, the abilities to control the light intensity and manipulate the propagation directions of the light become basic capabilities that support many optical excitation applications. Microfluidic systems can be utilized in the applications of biomedical screenings. For instance, bioanalyses [16] and manipulation of samples consisting of single cell or single molecule. The single cell studies are carried out by Craighead [17].

1.1.4 PDMS based optofluidic devices for lab-on-a-chip applications

In PDMS based optical systems, the light can be detected either based on pixel intensity or with optical fiber detection. It is possible because the PDMS material is

transparent and provides high degree of fluid manipulation capability within the microchannels [18]. These characteristics are crucial in the fabrication of microfluidic devices for biomedical applications. Some important capabilities of the PDMS based microfluidic circuits include highly localized laser excitation, integrated bio-chemical sensing, and single cell analysis.

Optofluidic compartments, together with biocompatibility of PDMS replications, enable a new approach of developing optofluidic technologies that can be readily integrated with lab-on-a-chip applications.

1.2 Literature review

1.2.1 Development of reflectivity based optical switch

There are many research efforts put into inventing the optical switch. Optical switch is a crucial component for changing the propagation direction of light. Most of the conventional optical switches cannot be integrated with microfluidic systems. Some of the recently reported optical switches can be integrated with lab-on-a-chip microsystems, holding much promise to advance optical switching technology in miniaturized biomedical systems. However, the integration of optical switches with planar microfluidic devices relies on the reduction of complexity in fabrication and the innovation in planar optofluidic circuits.

Sakata et al. [19] introduced the conventional thermocapillarity optical switch. It used microheaters to heat up the refractive-index-matching liquid. The heating led to the changes of the surface tension in the groove which the refractive-index-matching liquid resided. The change of surface tension moved the liquid at the middle point of the waveguide so that the light can be coupled into the crossing waveguide. It used the total internal reflection (TIR) to change the light propagation direction at the silica-air interface. The force driving the movement of the liquid was not huge. Consequently, the viscosity of the liquid was as low as possible. PDMS was chosen as the refractive-index-matching liquid. By controlling the weight-average molecular weight, the absolute viscosity of the PDMS could be controlled. The minimum switching time of 50-100 milliseconds was dependent on the minimum heating duration. The design of thermal capillarity optical switch could be applied to optical communication network. However, it could not be

applied in the lab-on-a-chip platform within the planar microfluidic circuit due to the complexity in fabrication processes.

Li et al. [20] investigated an optical switch driven by electro-optic phenomenon. It used a Y-shaped optical waveguide with one and two input waveguide. The optical switch was named digital photonic splitting switch (DPS) as the optical switching was achieved by altering the applied voltage. SiGe layer was used as the material to construct the optical waveguide. It used widened carrier injection regions at the output arms to reduce the switching voltage hence achieving lower power consumption. The refractive index difference between the silicon wafer and the SiGe provided the vertical confinement of the light. The ridge wall formed by silicon oxide and SiGe provided the lateral confinement of the light. The SiGe achieved different refractive index when the carrier concentration in this layer was changed. The increase of carrier concentration was achieved by forward biasing the SiGe layer. Electrons were injected into the p-region of the SiGe layer. This plasma dispersion effect lowered the refractive index of the SiGe layer which would cut off the light transmitting at that particular branch. The photonic splitting switch demonstrated involved complex fabrication process which cannot be integrated with microfluidic network.

With the research trend of microfluidic emerging, Campbell et al. [21] demonstrated the TIR technique of integrating the optical switch within the microchannels. The optical switching with switching speed of less than 20ms [21] was achieved by injecting two mixable fluids into the microchannels. The overall structure consisting two layers of microchannels was separated by thin flexible membranes and another layer for control channels. The flexible membrane served as pressure-controlled micro-valves. Three microfluidic channels were connected to

the membrane via two fluidic inlets and one fluidic outlet. The fourth microchannel and the vent in the flow layer aimed to purge the dead volumes between the microfluidic inlets and the mirror microchannels. The valves were driven by a controller, controlling the replacement of fluid within the microchannels. The critical angle was decided by the refractive index between the PDMS and the fluid injected. The viscosity of the fluid was maintained close to the viscosity of water to ensure the chip could perform fast switching under moderate pressure. The optical switch demonstrated can be integrated with microfluidic channels but the construction of the multiple layers of structures was complex. The chip switched the light in vertical plane which was perpendicular to the chip substrate [5][21]. This optical switching technique could not be integrated into the planar microfluidic circuit. Compared to the optical switch [19-20], this technique provided the possibilities to integrate optical switch in PDMS based lab-on-a-chip device with complex fabrication process.

In the attempt to miniaturize the optical switch with planar microfluidic devices, Wolfe et al. [22] reported a liquid core/liquid cladding optical waveguide. The liquid-liquid waveguide enabled the manipulation of light in the waveguide, which was formed by a core liquid fluid flow clamped by two liquid fluid flows. The liquid core-liquid cladding waveguide formed the laminar flow at the interface of the core-cladding fluids. The fluidic interfaces were optically smooth for the confinement of light within the centre core fluid. The light confinement had small optical loss. The liquids flowing inside the microchannels had Reynold number ranges between 5 and 500. The Reynold number was low and would not lead to turbulence. It ensured laminar flow between the liquid core liquid cladding fluid interfaces. The flow rates of the core and cladding fluids could be adjusted and

manipulating the compositions of the core and cladding fluids could alter the fluid properties. In the experiment of liquid core-liquid cladding waveguide [22], calcium chloride solution at refractive index of 1.445 was used as the core fluid while the cladding fluid was the deionized water with refractive index of 1.335. The refractive index difference between the core and the cladding fluids ensured that the light would be constrained within the core fluid. In addition, the PDMS with refractive index less than 1.445 would function as cladding in the waveguide. Microfluidic circuits for liquid-core liquid-cladding waveguide was modeled into an optofluidic switch by adding two cladding fluids to the inlets and three outputs to the fluidic outlets. The switching sequences could be realized by adjusting the differential flow rate of the cladding fluids. Four fluidic inlets were needed instead of two fluidic inlets because large differences in the cladding flow rates would result in the deformation of core fluid stream. This would cause the loss of light signal when the core fluid approached the splitting junction. The cladding fluids were used for constraining the width of the core fluid. The cladding inlets were for directing the switching sequences. The switching speed is 0.1 Hz.

Similar optical switching technique with pneumatic tuning mechanism was also reported by Lim et al. [23] with switching time of 30ms. These two optical switching techniques [22-23] provided optical switching capability in the horizontal plane which was parallel to chip substrate and seamless integration with microfluidic circuit. Switching angle was the angle between adjacent optical outlets. However, the switching angle between each optical output was less than 45°. The optical switch used liquid-liquid interfaces to guide light [22-23]. Liquid-liquid interfaces were inherently sensitive to external factors such as the change of fluid pressure or bubble formed within the microchannels. To increase the switching

angle and the switching versatility of the optical switch, more investigation was needed to create optofluidic switch that could solve this limitation. Furthermore, it would be another challenge to create an optofluidic device that could eliminate liquid-liquid optical interfaces at the same time increase the switching versatility.

1.2.2 Development of reflectivity based refractive index sensor

Refractive index sensing is useful for various biomedical and chemical diagnostic applications involving liquid substances. Surface plasmon resonance (SPR) sensor based on the Kretschmann system [24] was formed by three layers of material including glass, gold and air. The sample to be sensed was placed on the metal coating. This metal coating is coated on top on a prism and the light is reflected on this metal coated surface. At a specific angle, SPR occurred. By measuring the amount of reflected light, the sample's refractive index can be acquired. The sharpness and gradient of the SPR peak defines the sensitivity of the refractive index sensor. The sensing resolution of the refractive index is 1×10^{-6}. The fabrication process for the aforementioned Kretschmann system is complex which involved multilayer of thin films. The configuration of this sensor cannot be integrated with the planar PDMS devices.

Micheletto et al. [25] had shown theoretically that the sensing sensitivity at the critical angle is infinite. A less complicated device [25] compared to the Kretschmann system [24] was constructed by injecting laser light into a piece of glass at different angles to generate multiple reflections. The glass was immersed in the fluid analyte. The output light was detected by a planar detector. Diluted ethanol was used for the experiment. The sensitivity represented by a sharp peak at the critical angle provides the capability for fluid refractive index sensing. The

detection of the surface plasmon resonance at the critical angle yield high sensitivity. However, the system detected light in the plane perpendicular to the glass slide and it was not ready to be integrated with planar microfluidic circuit.

The integration of refractive index sensor with microfluidic circuit was demonstrated by Sarov et al. [26] with sensing resolution of 2×10^{-3}. This sensing technique was based on diffraction which happened during the TIR. The fabrication techniques for the chip included soft lithography, dry etching, PECVD and hot embossing lithography. The laser beam impinged on the prism facet with angle larger than the TIR angle. TIR occurred at the optical interface between the micro-prism and the fluid in the microchannel. Diffraction grating constructed between the prism and the microchannel was formed by metal lines and transparent lines. The diffraction grating pattern was affected by the angle of incidence and the change of refractive index of the fluid. The measurement sensitivity could be improved by altering the angle of incidence near TIR angle. However, the increase of measurement sensitivity came at the expense of a lower measuring range. The proposed sensing technique required complex fabrication processes which hindered its possibility to be integrated with planar microfluidic circuit.

In the attempt to integrate refractive index sensor into the planar microfluidic system, Brennan et al. [27] investigated the interference pattern formed by the reflection at the solid-liquid-solid interfaces. The interference pattern changed according to the refractive index of the fluid analyte. The Fresnel reflection occurred at low coupling angle at the liquid interface. When the coupling angle was between 0° to 42° and the refractive index of the liquid was low, the light was guided within the microchannel. But when the coupling angle was 42°, the light was fully reflected. When the refractive index of the liquid was 1.4, the change of

critical angle caused the occurrence of the interference pattern. The reflection period was depended on the microchannel height. When the interference phenomenon was observed, thin film reflectance measurement could be made under a single wavelength. The thin film separated the reflection and transmission region. It could achieve the refractive index measurement of 1.33-1.35 for liquid that was transparent and non-scattering with detection resolution of 1×10^{-6}. It would be useful to construct an optofluidic refractive index sensor with extended refractive index measurement range [25] while preserving the seamless integration with planar microfluidic circuit.

1.2.3 Development of reflectivity based microlens

Lenses are critical components in localized excitation or sensing applications. The optofluidic lenses aim to increase the light intensity at a particular position within the microfluidic circuit. For the solid lens, the geometry of the lens is permanently fixed. So the lens is unable to achieve optical tunability by reconfiguring lens profile. The previous methods to achieve focal length tunability involve complex fabrication processes for tuning methods involving hydraulic pressure [28], electrowetting [29], stimuli-responsive hydrogels [30], and redox surfactants [31]. These tuning schemes only provide optical tunability in the direction perpendicular to the chip substrate. Consequently, they lack the potential for integration with planar PDMS devices. To meet the challenge of optical focusing in planar PDMS device, hydrodynamically tunable optofluidic microlens was designed by Mao et al. [32] and Seow et at. [33]. The optical properties of the lens could be easily manipulated by the variations in the property of the fluids. The optical manipulations were based on microflows manipulation via the control of fluid flow

rates. Different lens shapes and curvatures could be achieved and tuned through the control of fluid flow rates. The formation of the optical interface was based on the generation of a pair of secondary counter-rotating vortices (Dean Vortices) [32]. The optical interface of the liquid lens [33] was formed by laminar flows within the expansion chamber. The liquid microlenses from biconvex lens, planar convex lens to concave convex lens [33] was obtained by adjusting the flow rates. The optical focal length was hydrodynamically tunable. Minimizing the diffusive broadening at the interfaces also eliminated the optical aberration with increase of optical intensity for 4.27 times compared to the unfocused light. The further advancement of the fluid based microlens with three-dimensional light focusing ability was reported by Rosenauer et al. [34]. Although the aforementioned microlens had ability to be integrated into the planar PDMS chip, the fluid-fluid interfaces were inherently unstable and sensitive to external factors which would disrupt the optical functionality. These external factors included the formation of bubbles within the microchannels and the change of fluid pressure. The formation of fluid-fluid interface needed the continuous supply of fluid which would considerably shorten the life time of the optofluidic devices. Consequently, there was a need to create an optofluidic circuit that could perform more optical functionalities while eliminating the aforementioned disadvantages.

1.2.4 Microfluidic manipulation technique as optofluidic basic tuning mechanism

In cytometry approach [35], cell sorting and profiling are realized. However, the cost of building a system based on the cytometry approach is high. It involves focused laser beams, control circuits, and optical detecting and filtering devices. Fluorescent activated cell sorting (FACS) uses cells that are labeled with

fluorescent dye. The dye targets specified cells that have antigens bonded on it. The stream of cells passing through a vibrating mechanism breaks it into individual droplets. Each droplet will have a cell inside. The probability of having two cells in a single droplet is comparatively low. Right before the stream of cells break into micro-droplets, the fluorescent detection system picks up the signal in the form of electrical charges. One of the components that is responsible for signal detection is an electrical charging ring that is placed right at the point where the stream breaks into droplets. However, if the sample stream has contamination, the accuracy of measurement will be low. Due to the cost and complexity of the cytometric system, there is a need for a low-cost device that can function as cell sorter. One of them is termed hydrodynamic focusing that can accomplish the same sorting and detection purposes. The hydrodynamic focusing is created from the interest to mimic the function within the cell cytometer as its application. After the stage of hydrodynamic focusing, the sample cells will undergo the stage of cell detection. Several methods were introduced for cell detection including electrochemical detection [36] and fluorescent detection [37]. The most popular method is by fluorescent detection. Its advantage includes high sensitivity even when the sample volume is small. Under fluorescence detection, the laser excites the species. After a period of time, the excited species will emit a wavelength, which is larger than the excitation wavelength. The emission light is measured as detection signal. Another advantage of fluorescent detection lies in one of its properties. Fluorescent's signal is isotropic. The fluorescence emission is three-dimensional. It is possible to obtain either two dimensional or three dimensional images from the fluorescent detection. Fluidic transportation system consists of fluidic drivers that generate fluid of hundreds of microliters per minute. These methods include hydraulic pressure and

electrokinetic force [38-40]. Other pumping method that has been reported before is electrohydrodynamic [41].

There are also other methods that can achieve fluid delivery via eletroosmotic and electrophoretic transportation [42]. Pressure driven flow using hydraulic pressure is commonly used for delivering fluid into microfluidic system. In microfluidic based fluid delivery system, ideally if two fluid streams met at the junction of the microchannels, they will flow in parallel without eddies or turbulence. There is minimal diffusion at the interface between the two fluids. The objective of hydrodynamic focusing is to provide sheathing for the core stream. It ensures that the cells within the core fluid only travel within a very narrow field of view. In hydrodynamic focusing, ideal laminar flow [17] is predominant. Laminar flow prevents premature mixing of cladding and core fluid streams. The first generation of the hydrodynamic focusing chip provides focusing on two dimensional planes. Due to the fact that it didn't provide hydrodynamic focusing in vertical plane, it causes the variation in signal detections and variation in speeds at different vertical locations. In planar view, the traveling of beads or cells is either at top or bottom of the channel. Consequently, for cells that travel out of the focal plane of detection, low signals are detected. Cells at different height will also acquire different speeds, which will lead to measurement errors during the optical detections. A uniform velocity profile for all cells is preferred. The second generation of focusing structure aims to achieve focusing that can sheath the core flow vertically [43]. The aim of hydrodynamic focusing is best realized at small length scales. Small length scale also has distinct advantage for mass-fabrication to produce cheap and disposable devices.

Turbulence accelerates mixing and enhances diffusion. Turbulence can happen by forcing reactant streams at high velocity through a nozzle. This method is inherently hard to control and usually consumes large volume of samples [44-45] and imposes dead time. Dead time is undesirable because the reaction is obstructed from view during dead time. Microfluidic prevents these conditions by shortening the length scale over which the fluid diffuses. It provides capability of reducing dead time by allowing the mixing or optical light path within the microchannel to be monitored. Microfluidic can be viewed as a continuous flow mixer capable of achieving mixing time of shorter than 10 μs without inducing turbulence. A fast mixing time and small sample consumption rate are the advantages of hydrodynamic focusing in small length scale. Hydrodynamic focusing can assist in cell sorting of cellular metabolism on single cell level [46-47]. The first generation of the proposed structure consists of four rectangular channels; 10 μm deep and wide, intersecting at the center. Fluid from fluidic inlet is labeled with fluorescent dye. To achieve focusing at the center, cladding fluids flow from side channels, thereby squeezing the core fluid. Adjusting the fluids pressure at inlet and side channels can vary the core fluid's width. The time resolution is related to the flow speed. When the flow speed yields better than a microsecond per micron in travelled distance, the microchannels still ensure laminar flow. The hydrodynamic focusing minimizes the sample volume consumed by the mixer. Compared to the turbulent mixer, the volume flow of hydrodynamic focusing is slower over three magnitudes, reaching a scale of nanoliters per second [46-47]. The hydrodynamic focusing structure can be modeled by an equivalent circuit model [48]. The microfluidic manipulation technique of focusing microchannels possesses tunability in the width of the core fluid. Hence the fluid manipulation technique becomes the fundamental mechanism

that is used in the following chapter to realize optofluidic switch as another application of hydrodynamic focusing.

1.3 Fabrication technology for micro-total-analysis-system

1.3.1 Overview of μ-TAS fabrication technology

MEMS microfabrication technology has realized the μ-TAS systems. μ-TAS involves sample execution, sample transportation, reaction, separation and detection. μ-TAS technology [18] aims to reduce the size and cost of this crucial instrument for many biomedical applications including cell sorting and detection. Various materials have been chosen for the fabrication of MEMS and μ-TAS devices. This microfabrication processes can be applied to metal [49-50], silicon [51-53], glass [54-55] and plastic [56-60]. The microfabrication technology originated from MEMS has enabled the fabrication of microstructures as the microfluidic systems on the silicon mold.

The current silicon fabrication technology has advanced to nanometer regime using electron beam scanning. However, the first generation silicon fabrication technology in micron regime for MEMS fits well in the fabrication of silicon mold for μ-TAS devices. The microfluidic channels typically have widths of 10-100 μm. Consequently, in the current trend of microfluidic miniaturization, silicon fabrication technology derived from conventional MEMS lithography is being utilized as the standard fabrication process. It provides a faster, less expensive method to fabricate the microstructures on the silicon mold as the rapid prototyping process. Once the silicon mold is fabricated, PDMS casting and peeling process is conducted as replica molding process. The combination of these two processes

allows microfluidic systems to be designed and fabricated rapidly and inexpensively. Replication by PDMS casting and peeling becomes an important rapid prototyping method in producing state-of-the-art microfluidic chip based on polymeric material. It has characteristics of high replication fidelity for microstructures, low curing temperature, non-toxicity and reversible deformation. It also provides reversible sealing between PDMS or other materials via molecular contact with the surface and irreversible bonding after exposure to air plasma via formation of covalent bonds. PDMS has controllable surface chemistry, smooth surface and repeatable casting and peeling process without damaging the structured silicon wafer. The unmodified PDMS has hydrophobic surface but it can be rendered hydrophilic in the presence of silanol groups. The surface modified PDMS has greater resistance towards adsorption of hydrophobic and negatively charged analytes. PDMS represents a suitable material for electro-osmosis (EOF) and pressure driven flow. This replica molding process is easy to fabricate under bench top condition, which does not need to be made under the clean room environment. The PDMS material provides smooth vertical sidewalls in the microchannels, which are crucial for light to transmit through, or to be confined within the microchannels. Within a single pass of lithography, these optofluidic compartments can be integrated with other microfluidic functionalities. Take for instance, the single cell-sorting combines light source and optical sensing for bio-sensing applications. The silicon mold that requires a single layer lithography exposure can be fabricated followed by PDMS casting and peeling which reduces the production time to a single day. Furthermore, tens of chips with different designs can be made simultaneously on a single standard p-type < 1 0 0 > 4 inches silicon wafer. This greatly improves the efficiency and flexibility in designing the silicon layout.

Different parameters in the design can be implemented easily for optimizing the performance of the device's functionality. PDMS microchannels have the disadvantage of susceptibility to particles with size comparable to the microchannel's width. The particles would induce clogging within the microchannels. However, this problem can be avoided by filtering the fluids before being injected into the microchannels. The inherent properties of PDMS enable the integration of tunable optical components into adaptive optical detection systems. These properties are essential in realizing integrated micro-optical-fluidic-systems (MOFS). The microfluidic systems inherently have the advantages of decreasing the cost in manufacturing, reduction of time for chemical analysis, reduction of fluid analyte consumption and increase portability. PDMS devices obtained from micro fabrication process possess optical properties and surface chemistry that are suitable for various biomedical devices.

1.3.2 Standard soft lithography fabrication process

The microchannels are made on a four inch < 1 0 0 > p-type silicon wafer using standard soft-lithography process. Firstly, the silicon wafer is immersed in ethanol for ten minutes. Secondly, it is washed with isopropanol for three minutes for three times. The silicon wafers are blown with pressurized air and put in the oven at 120°C for duration of 20 minutes to remove any moisture resides on the wafer's surface. A layer of SU-8 50 photoresist is laid on the silicon wafer by spin coating. The spin speed is 500rpm in the first ten seconds which is then ramped up to 1900rpm for thirty seconds for the photoresist to be evenly distributed onto the silicon wafer. The coated silicon wafer is put into the oven again for removing the water component in the photoresist. The temperature within the oven is set at 65ºC.

The coated silicon wafer is placed in the oven for 150 minutes. After 150 minutes, the silicon wafer is allowed to cool down in room temperature after duration of 20 minutes. The dried silicon wafer with SU-8 50 coating having thickness of 80μm is put in the Suss MicroTec MA8 lithography machine for UV exposure. This lithography machine has an exposure wavelength of 365nm and exposure density of $6mWcm^{-2}$. For the SU-8 50 photoresist with thickness of 80 μm, the required exposure dose is $470mJcm^{-2}$. The exposure time for the SU 8 photoresist coated wafer is set at 78 seconds to achieve the required exposure dose. After the UV exposure is completed, the photoresist that is shined by UV is crosslinked. To further enhance the crosslinking process, the UV exposed wafer is put in the oven which is set at 65 ºC for five minutes. The temperature in the oven is increased up to 95 ºC for subsequent ten minutes. After the post-exposure baking at 95 ºC, the wafer is allowed to cool down to room temperature for forty five minutes before it is developed with SU-8 developer. During the development process, the microstructures should be clearly visible on the silicon wafer. The developed SU-8 microstructures are washed by isopropanol to remove the residual of the photoresist. The fully cleaned wafer with microstructures is blown with compressed air and put in the oven at 65 ºC for ten minutes. The oven's temperature is then increased to 120 ºC for forty minutes to enhance the crosslinking process. After forty minutes, the wafer is allowed to cool down to room temperature in ninety minutes. The purpose of this step is to prevent the forming of microcracks within the SU-8 microstructures. The wafer with microstructures is placed in a mold to be filled up with PDMS. The PDMS elastomer (Sylgard 184 Silicone Elastomer Kit) is mixed with the curing agent at 10 to 1 weight ratio. After the mold is filled with PDMS with the fabricated wafer at the bottom, the PDMS is degassed to remove the

bubbles residing within the PDMS. The mold containing the PDMS is put in the oven at a temperature of 100°C for sixty minutes for curing. The refractive index of the PDMS after the curing is 1.43. The microstructures on the silicon wafer are imprinted onto the PDMS slide and become microchannels. The fabrication resolution of the quartz mask is 3 μm. The microstructures on the wafer have the smallest width of 30 μm. Consequently, the microchannels' sidewalls are optically smooth which will reduce the optical losses at the fluid-solid interface. One piece of PDMS slab is fabricated with microchannels imprinted on it. 0.5mm holes are drilled through the PDMS slab for connecting to the fluid dispensing system via microfluidic inlets and outlets. The surfaces of the transparent glass and the PDMS slab are cleaned and rendered hydrophilic by plasma surface treatment (March plasma system PX-250, March Instruments Inc.) before bonding together. This fabrication process will be applied in every subsequent chapter to fabricate the optofluidic chip.

1.4 Research objective and scope of study

A lot of research effort has been invested to create light manipulation devices. However, most of these devices are made for free space optical coupling which cannot be integrated with PDMS microchips. There are fewer reported studies dealing with incorporation of light manipulation capabilities into planar PDMS devices. The miniaturization of the light manipulation devices down to micrometers scale also brings the benefits of seamless integration of microfluidic circuits with optofluidic circuits, for instance, the on chip fluorescence and refractive index sensor. The aforementioned benefits include optical tunability and reduction of fluid consumption.

Systematic investigations are needed to achieve optical light switching, different proportion of light distribution, diverging, collimating and focusing in optofluidic devices. The optical performances of each optofluidic devices catering to different optical functionalities have to be characterized.

The objectives of the thesis are as followed:

1. To study the tuning of refractive index mismatches at fluid-fluid interfaces and solid-fluid interfaces to achieve tunable optical switching, divergence, collimation and focusing in planar PDMS microchip for seamless integration with microfluidic circuits.
2. To eliminate all mechanical components while achieving micro optical manipulations.
3. To prolong the life time and optical stability of the optofluidic device without sacrificing optical tunability by eliminating fluid-fluid optical interfaces. The life time is the amount of time the optofluidic devices can function before the fluids are fully consumed.
4. To achieve optical sensing in MOFS by investigating effects of the change of the material properties of the fluid analyte towards the optical reflectivity of the solid-fluid optical interface.

The scopes of the study are as followed:

1. The research emphasizes on the study of microflows and the optical reflectivity characteristics of the fluid-fluid interfaces. All the fluids used in the experiments are assumed to be Newtonian fluids with constant viscosities.

2. Secondly, the thesis focuses on the study of the optical reflectivity of the solid-fluid interfaces used in applied optics for light manipulations. The solid-fluid interfaces are transparent. The surface roughness of the PDMS is measured at 2 nm by the atomic force microscope (Bruker, Dimension FastScan).

1.5 Organization of the thesis

This thesis is divided into six chapters

Chapter 1 includes the introduction part of this thesis, including the research background, literature review, research objectives and scope.

Chapter 2 uses the hydrodynamic focusing mechanism illustrated in chapter 1.2.4 to realize micro-optical switching with optofluidic circuits using fluid-fluid optical interfaces.

Chapter 3 addresses the disadvantages of limited life time and low mechanical stability of the fluid-fluid interfaces for the optofluidic switch by utilizing cascading prisms. The optofluidic switch based on cascading prisms also increases the available switching positions compared to the optofluidic switch discussed in chapter 2. Fluid-fluid optical interfaces are replaced by solid-fluid interfaces for light switching.

Chapter 4 involves the study of the optical partial refraction phenomenon observed in the previous chapters when the light is switched from one optical outlet to another. Optical partial refraction was observed when part of the light has incidence angle larger than critical angle, while part of the light has incidence angle smaller than the critical angle. The studies of the optical reflectivity led to the development

of refractive index sensor used for sensing the refractive index of the fluid without the need to label the fluid analyte.

The optical phenomenon observed from Chapters 2-4 is based on the change of optical reflectivity on flat optical interfaces. Chapter 5 describes the change of optical reflectivity using a curved surface to investigate tunable optical focusing, diverging, and collimating.

Finally, Chapter 6 presents the conclusion and several recommendations for future works.

Chapter 2

Tunable optofluidic switch via hydrodynamic control of laminar flow rate

2.1 Conceptual design and working principle of the tunable optofluidic switch

There are inherent drawbacks of the electro-optics switch [61-62] that render it unable to be incorporated into PDMS based chip. The fabrication process for the electro-optics switch is not compatible with the soft lithography process usually employed for the making of microfluidic circuit. Consequently, the optical switching functionality of the electro-optics switch cannot be realized in the PDMS based microfluidic chip. It is unable to function as part of the multi-purpose integrated microfluidic system. Utilizing the characteristic of the laminar flow, light switching can be achieved by innovatively combining tunable fluid-fluid interface via hydrodynamic focusing with angled placement of input optical fiber. This configuration will promote TIR [63]. The hydrodynamic focusing that is based on the tuning of liquid-core liquid-cladding has higher refractive index for the core liquid and lower refractive index for the cladding liquid. The optical switching is achieved by adjusting different flow rates of the three fluid inlets. By varying the flow speeds of the three laminar flow streams, the width of the core fluid can be altered. The change of the width of the core fluid is essential in realizing optical switching. The optical switching is realized in one dimension in the horizontal plane parallel to the microchip surface. There is no difference in optical intensity at

different vertical height of the microchannels. Consequently, the proposed light switching technique does not include three-dimensional light focusing capability. The microchannels for hydrodynamic focusing are streamlined at the intersection of three fluid inlets to promote higher stability of the laminar flow and less ionic diffusion. Stable laminar flows will help the formation of smooth liquid-liquid interfaces for TIR.

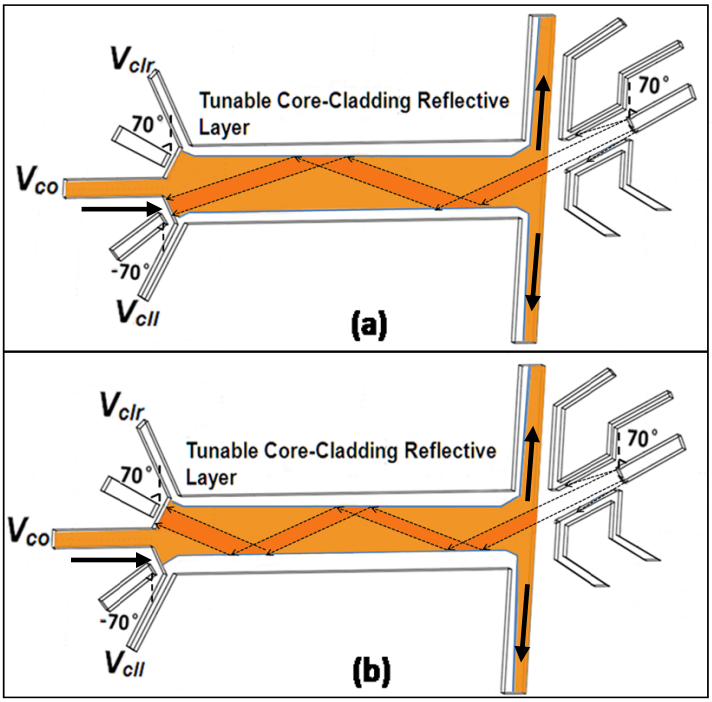

Figure 2.1 The hydrodynamic tunable optofluidic switch with its two corresponding switching positions

Figure 2.1 depicts the schematics of both the switching positions of the tunable optofluidic switch. By maintaining the upper fluid-fluid interface and raising the lower fluid-fluid interface, the lightpath is altered via TIR to realize the optical switching. This transition can be achieved by increasing the flow rate V_{cll} at faster pace compared to V_{clr} while maintaining flow speed of the V_{co}. The core fluid is combined with the upper and lower cladding fluids at the cross intersection. When the V_{cll} and V_{clr} flow at the same flow rate, the core fluid V_{co} has to be injected into

the focusing structure with sufficient flow rate to maintain the sufficient width of the core fluid for the laser beam to be coupled into the core fluid. To confine the light within the core fluid, the refractive index of the core fluid needs to be higher than the cladding fluid. The core fluid has a refractive index of 1.43 while the cladding fluid has a reflective index of 1.33. The total TIR of 68° can be calculated from the mismatch of refractive index between the core and cladding fluids. The input optical fiber is placed at an angle of 70° measured vertically. The laser beam would impinge on the fluid-fluid interface at angle that is 70° or more than 70°. The light that is equal or more than 68° would meet the criteria of the critical angle and will undergo TIR.

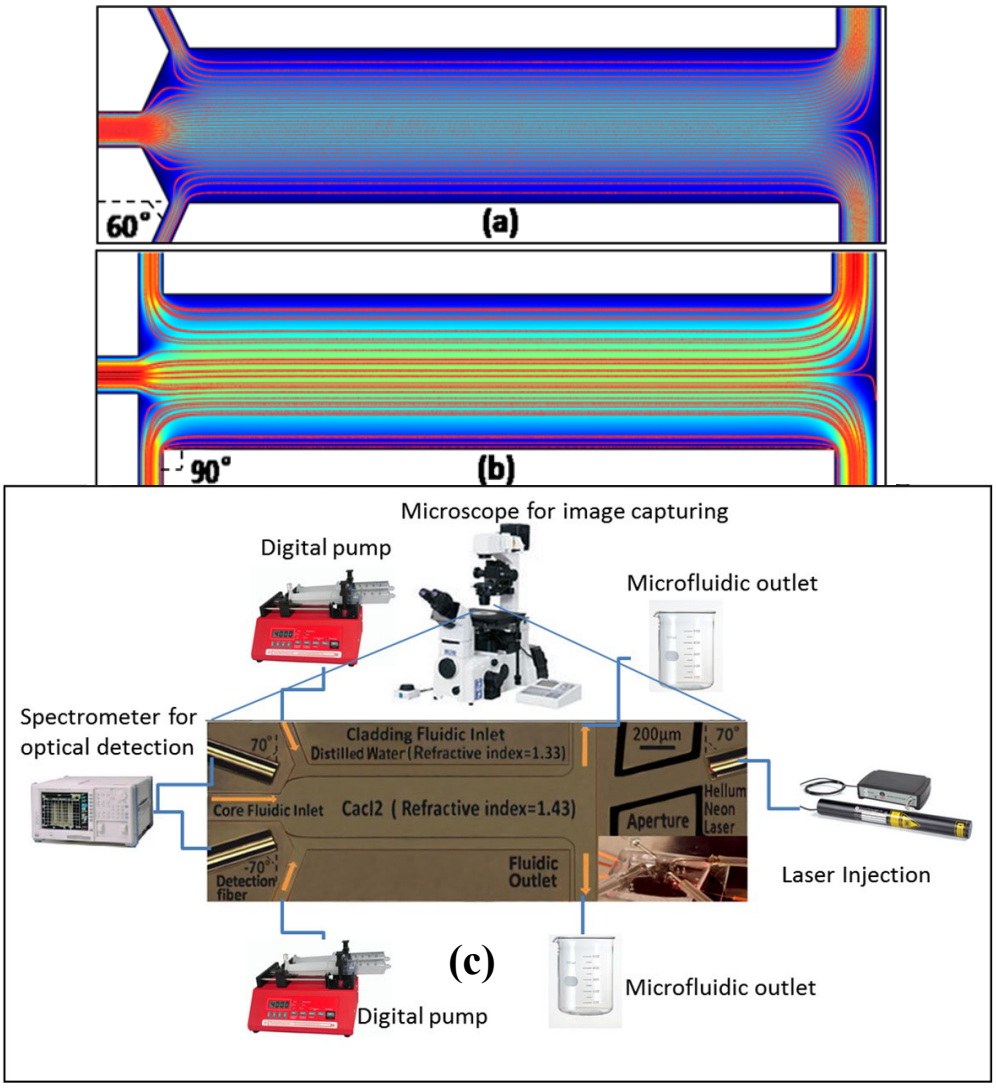

Figure 2.2 (a) Hydrodynamic focusing structure with 60° injection angle

(b) Hydrodynamic focusing structure with 90° injection angle (c) optofluidic circuit for hydrodynamic tunable switch

The hydrodynamic focusing structure is designed with tapered angle fiber insertion cavity for optical detection. The tapered angle design in Figure 2.2 with 60° injection angle provides wider core liquid if we compare the simulation results of Figure 2.2(a-b) under the same flow rates. The hydrodynamic focusing structure in Figure 2.2(b) utilizes 90° injection angle. The 2D planar simulation results are calculated based on incompressible Navier-Stokes equations using Comsol Multiphysics simulation software. The simulation results show that laminar flows can form in the hydrodynamic focusing structure with or without the 70° injection angle. The three fluid streams flow out of the microchip via two fluid outlets. The streamline and the color within the microfluidic channels depict the velocity profiles of the laminar flow streams. Wider core liquid is helpful for the light to be coupled into the liquid core. Liquid core that has insufficient width makes the optical coupling partial and incomplete due to multiple refractions at the fluid-fluid interfaces before the light undergoes TIR. Secondly, the tapered angle helps to form laminar flow streams which are beneficiary in forming optically smooth fluid-fluid surfaces for undergoing TIR. The tapered angle design in Figure 2.2(a) with 60° injection angle also provides perpendicular coupling surfaces which minimize refraction before the light impinges on one of the two optical detection fibers.

2.2 Optical experimental setup for the optofluidic circuit

The widths of the microfluidic channel for core fluid and cladding fluid inlet are 150 μm and 75 μm, respectively. One core fluid inlet and two cladding fluid inlets are combined at an intersection of the subsequent microfluidic channel. The microfluidic channel situated right after the core-cladding intersection has the width of 500 μm and length of 2700 μm. The core and cladding fluids flow out of the

microfluidic chip via two microfluidic outlet with a width of 150 μm. The profilometer shows that the microchannels have a uniform height of 80 μm. To detect the light that can fulfill the criteria for TIR, two optical fibers are placed at both sides of the microchannel for the core fluid. A pair of multimode fiber is aligned on two sides of the core fluid inlet. The multimode optical fibers are placed with an angle of 70° measured from the vertical axis which is perpendicular to the direction of the flow. The optical fiber that is connected to the light source is measured 810 μm away from the microfluidic outlet channel. To reduce the width of the diverging laser beam, a micro aperture containing black ink within is situated in between the input optical fiber and the microchannels outlet. The micro aperture will block a portion of the laser beam with higher divergence angle. The optical fiber for optical detection is connected to a high-resolution spectrometer (AQ6317C, Yokogawa Inc). The input optical fiber is coupled with the light source of He-Ne laser having wavelength of 632.8 nm and optical intensity of 150 mW (05-LHP-991, Melles Griot) as shown in Figure 2.2(c). The output fibers are coupled to a high-resolution spectrometer (AQ6317C, Yokogawa Inc) for light detection. The centre core fluid stream is $CaCl_2$ solution (RI = 1.43), which is mixed with hollow glass spheres having diameter of 10μm (Dantec Dynamics) for producing visible lightpath within the microchannel. The cladding fluids used for lower and upper claddings are distilled water with a refractive index of 1.33. The refractive indexes of $CaCl_2$ solution and distilled water are measured by Digital Hand-Held Refractometer (Reichert, AR200). The higher refractive index for the core fluid is utilized to constrain the light within the core fluid. The experimental images are taken by inverted microscope (TE2000-E, Nikon) with charge-coupled digital camera (DMX1200C, Nikon). The inverted microscope is focused on the

central height location to obtain clear optical images and reduce measurement errors. The width of the core fluid is calculated by choosing two points along the liquid-core liquid-cladding interface for two interfaces and measuring the distance between them. Each measurement for the width of the core fluid is performed five times to obtain an average value in Matlab (MATLAB 7.0 R14). The largest microchannel length of 2700μm divided by microchannel height of 80μm is 33.75. The fluid injection is realized by connecting the digital pump and the PDMS chip via silicon tubing (06411-59, Cole Parmer). Subsequently, the luer to carb connector (CX-012X, CONNEX) is connected to the tube (5212-B-90, EFD). The flow speeds can be adjusted using the digital pump.

2.3 Microfluidic tunability of the fluids within the microchannel

The hydrodynamic focusing structure is capable of tuning the width of the core fluid by varying the differential flow rates between the core and cladding fluids. The capability of the hydrodynamic focusing structure is shown in experiment and simulation results. The results obtained from the FEMLAB simulation (Comsol Multiphysics) closely approximate the experimental results.

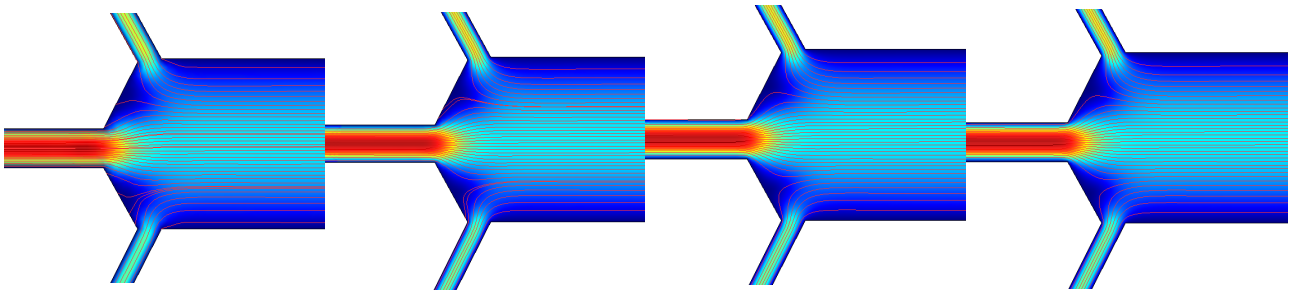

936 elements 3744 elements 14976 elements 59904 elements

(a)

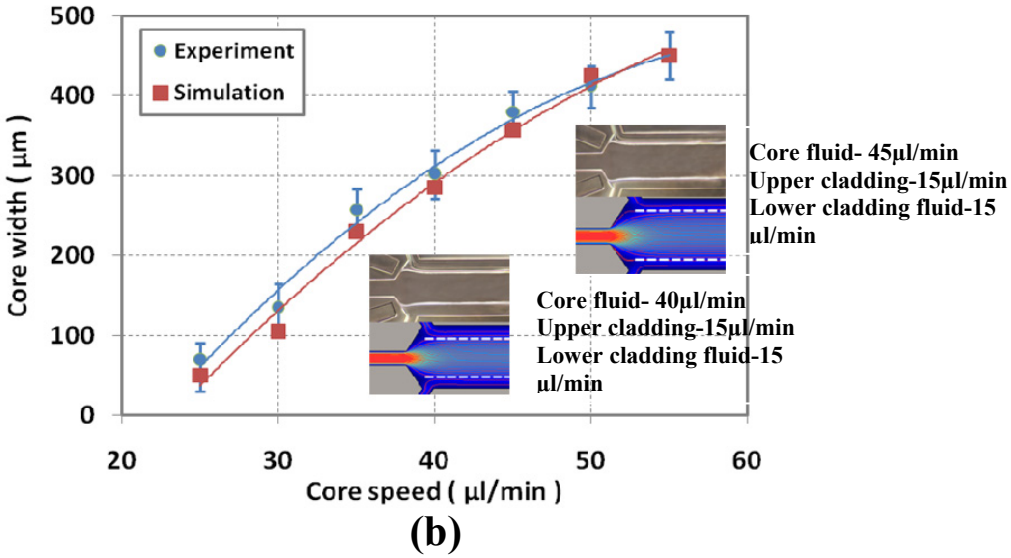

(b)

Figure 2.3(a) Convergence test of hydrodynamic focusing (b) Microfluidic tunability of the core fluid

The element used in the simulation is Lagrange – P2 P1. The simulation model in Figure 2.3 is the same as the simulation model in Figure 2.2(a) utilizing the same type of element. The number of elements in the simulation results in Figure 2.3 is fixed at 936, 3744, 14976 and 59904 for the convergence test. For the simulation result with number of elements of 936, there are flow lines that are originated neither from the core nor cladding fluid inlets due to the insufficient meshing density. When the meshing density increases, every flow line is originated either from the core or cladding fluid inlets. The core fluid's width stabilized and converges at 225 µm in the simulation model with 14976 elements. The core fluid's width does not change in both cases when the number of elements increases from 14976 to 59904. The simulation convergence testing is shown in Figure 2.3(a) when the core fluid flow speed is fixed at 35 µl/min while the upper and lower claddings are fixed at 15 µl/min. By varying the flow rates of the core fluid stream, the width of the core fluid stream can become tunable according to the experiment and simulation results shown in Figure 2.3. The width of the core fluid is measured thrice experimentally and the average value is obtained to verify the repeatability of

the experiment results. Second order polynomial is utilized for curve fitting all the data points for both the experimental and simulations results. The flow rate of the upper and lower cladding fluid is fixed at 15 µl/min, and increase the flow rate of the core fluid stream from 25 µl/min to 55 µl/min, the width of the core fluid increases from 70 µm to 475 µm. The width of both the upper and lower cladding fluid reduces in the same quantity when the width of the core fluid increases. The core fluid flow rate gradually increases at the interval of 5 µl/min.

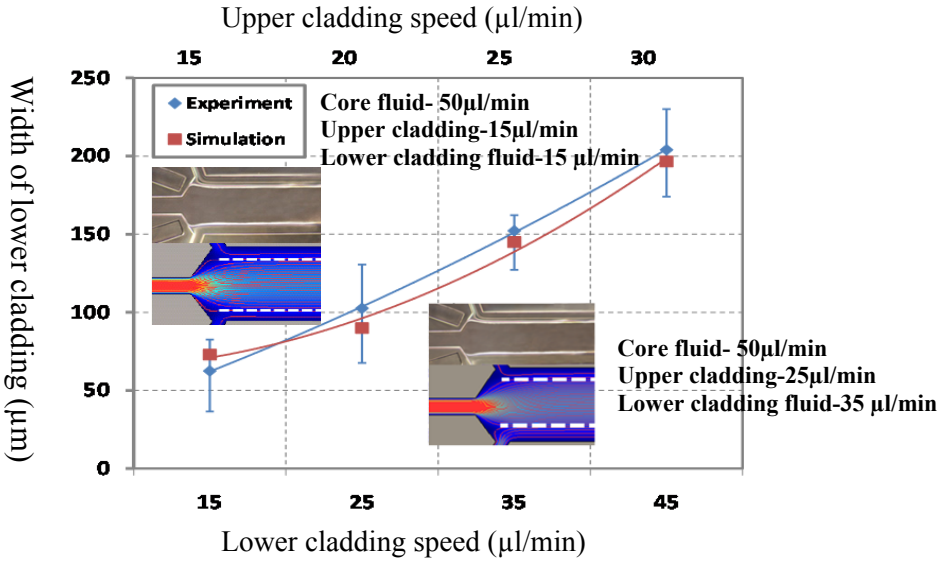

Figure 2.4 Microfluidic tunability of the lower cladding fluid

The hydrodynamic focusing structure also can maintain the width of the upper cladding fluid while increasing the width of the lower cladding fluid individually. The width of the lower cladding is measured from the liquid-core liquid-cladding interface to the sidewall of the microchannel. By tuning the different combinations of the flow rates of the lower cladding and upper cladding, the width of the lower cladding fluid stream can be tuned accordingly. The gradual increase of the width of the lower cladding fluid stream according to different combinations of fluid flow rates is shown in Figure 2.4. During the increment of the width of the lower cladding, the width of the upper cladding fluid stream remains the same. Similarly, each measurement for every combination of flow rates is repeated thrice to obtain

the average width of the lower cladding fluid stream. The experimental and simulation data are fitted on a curve by second order polynomial. The increase of the width of the lower cladding fluid stream is achieved by fixing the flow rate of the core fluid stream V_{co} at 50 μl/min. Meanwhile, the upper cladding flow rate gradually increases from 15 μl/min to 30 μl/min at an interval of 5 μl/min. The flow speed of the lower cladding fluid stream increases from 15 μl/min to 45 μl/min at an interval of 10 μl/min. The increment speed of the fluid flow rate of the lower cladding is faster than the upper cladding fluid flow rate. Consequently, the width of the lower cladding increases from 63 μm to 204 μm. After the liquid-core liquid-cladding laminar flows are stabilized, the width of the core fluid stream can be increased or decreased at the rate of 78 μm per second.

2.4 Experimental results of the optofluidic tunable switch with ZEMAX simulation results

The different combinations of flow rates of the upper and lower cladding fluid streams have led to the increase of the width of the lower cladding fluid while maintaining the width of the upper cladding fluid as shown in Figure 2.5(a-b). The increase for the width of the lower cladding has led to the optical switching of the laser beam from the -70° optical fiber to the 70° optical fiber at the optical detection outlets. When the laser beam is switched to the -70° optical fiber, the width of the lower cladding fluid stream is 75 μm. The optical intensity is reduced by 23%. Meanwhile, the laser beam width at the optical output fiber has an increment of 26%. In Figure 2.5(b), when the laser beam is switched to the 70° optical fiber at the optical detection outlets, the width of the upper cladding fluid stream is 125 μm. The optical intensity at this switching position is reduced by 42%. Meanwhile, the

laser beam width at the optical output fiber increased by 46%. The loss in optical power is proportional to the number of times of reflection the laser beam undergoes. The non-perfect collimated laser beam would produce laser beam with greater and greater amount of divergence when it undergoes more and more TIR. This would cause the loss in optical power. The fully collimated laser beam would reduce the divergence of the beam hence reducing the loss in optical power after the laser beam undergoes optical switching. The optical path length of the first ray of light entering the microchannel with 70° injection angle is 1177 μm, which is close to the optical path length of 1200 μm for the light with same injection angle obtained in the ZEMAX simulations. The experimental results exhibit close agreement with the simulation results obtained by TIR optical simulations (ZEMAX-EE, Leadintex International). The simulation results show that the micro-light switching capability can be realized if the light within the core fulfills the criteria of TIR.

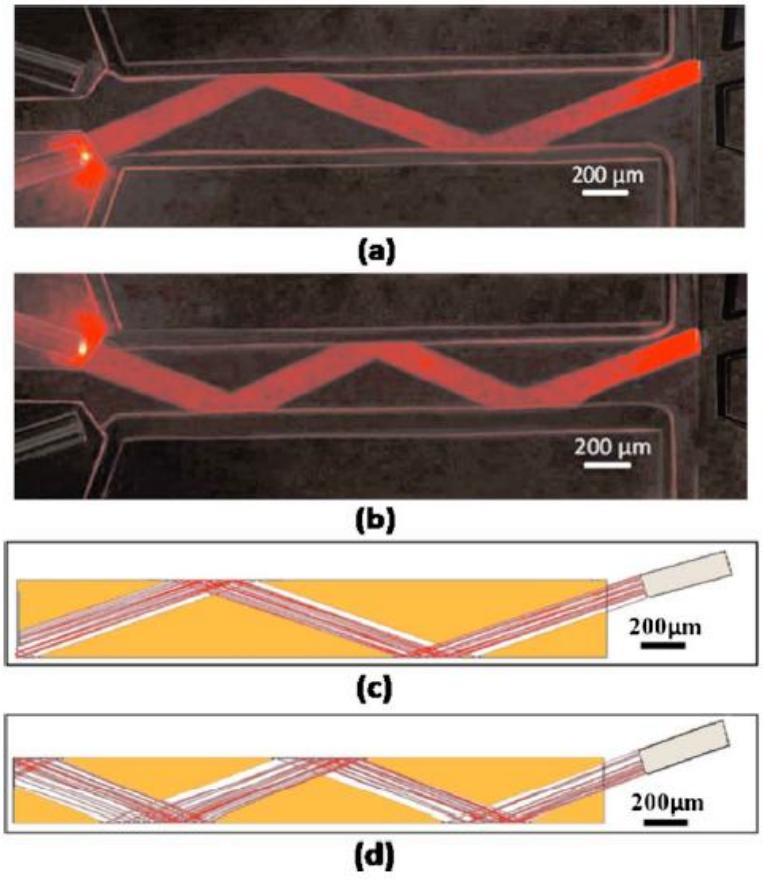

Figure 2.5(a-b) Optical experiment pictures of the hydrodynamic tunable optical switching, (c) Lightpath for the switching sequence (Zemax optical simulation)

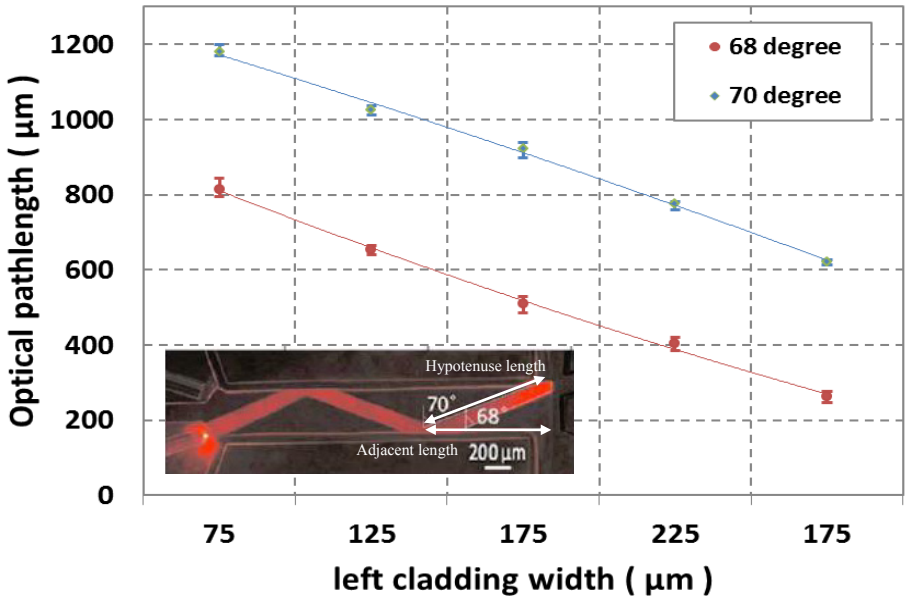

Figure 2.6 Optical path lengths with respect to the width of the lower cladding fluid at two different incident angles

Optical path length is defined as the length of the first ray of light that enters the microchannel before it impinges on the fluid-fluid interface. No optical refraction occurs when the laser beam that transmitted from PDMS to $CaCl_2$ solution as both of them share the same refractive index of 1.43. As the width of the lower cladding increases, the optical path lengths for light ray of 68° and 70° decrease as shown in Figure 2.6. The refraction angles of 68° and 70° are measured by calculating the injection angles based on the trigonometry calculations. For the 70° injection angle, the hypotenuse length is 1177 µm and the adjacent length is 1106 µm, respectively. For the 68° refraction angle, hypotenuse length is 765 µm and the adjacent length is 709 µm, respectively. The hypotenuse and adjacent lengths are measured by magnifying the Figure 2.5(a) by five times and measuring them according to the scale bar. The highest population standard deviation for the measurement of the optical pathlength is 19.90. Take for example, when the lower cladding width is 275 µm, the 68° optical pathlength measurements are 276 µm, 273 µm, 270 µm, 250

μm and 246 μm. The population standard deviation is calculated to be 12.46 for the sample size of 5. By magnifying the experiment photos by five times and measuring them with the scale bar, the highest measurement error for the width is 6.25 μm.

The reduction of optical path length is 551 μm from 814 μm to 263 μm for light ray with 68° incidence angle when the width of the lower cladding increases from 75 μm to 175 μm. Similarly, the optical path length with 70° incidence angle reduces by an amount of 557 μm from 1179 μm to 622 μm when the width of the lower cladding increases from 75 μm to 175 μm. The purpose of measuring the optical path lengths is to correlate the increase of the width of the lower cladding with the reduction of the distance the light travels before the first TIR.

2.5 Recommendation and conclusion

There are several unique advantages possessed by the hydrodynamic tunable optical switch. The hydrodynamic tunable switch provides optical switching functionality based on tuning of the fluids' flow speeds. The hydrodynamic tunable optical switch can be integrated seamlessly with many microfluidic functionalities as an on-chip device which its conventional solid counterpart [64-65] cannot achieve. The hydrodynamic tunable optical switch is fabricated using standard soft lithography process, which only involve a single time of exposure in soft lithography to create microstructures with uniform height. Consequently, other microfluidic circuits can be designed and fabricated alongside the hydrodynamic tunable optical switch for direct integration with its potential applications. In a four-inch wafer, many microfluidic chips can be fabricated at once which hasten the rapid prototyping process and lower the fabrication cost for each microfluidic chips. It can be integrated in microfluidic circuit for detection of fluorescence signal and bioassays

applications that is based on optical sensing. The distance between the two detection optical fibers is 360 μm. The hydrodynamic tunable optical switch is able to perform optical switching in micron scale. As the smallest resolution of the quartz mask is 3 μm, the fabricated microchannels' sidewalls are optically smooth, hence minimizing the optical scattering occurring at the solid-fluid interface. The Reynold number calculated based on the maximum combined flow rate within the microchannel for the hydrodynamic tunable optical switch falls in the range of 2.37 and 5.39, which lead to the elimination of diffusion at the fluid-fluid interfaces. If the combined flow speed is increased even higher, the Ca^{2+} and Cl^{-} ions have shorter time to diffuse over the same length within the microfluidic channel. The laminar flows for the three fluid streams ensure that the fluid-fluid interfaces are optically smooth without diffusion. This reduces the refractive index contrast between the core and cladding fluids. The time taken for the width of the lower cladding fluid to increase from 75 μm to 125 μm to complete the optical switching determines the optical switching speed. The optical switching is achieved by (i) forming the laminar flows for optically smooth fluid-fluid interfaces, (ii) injection of laser beam with angle of incidence larger than critical angle, (iii) creating refractive index difference at the liquid-core liquid-cladding interfaces and (iv) the tuning of the position of reflective surface via control of the flow rates. The refractive index variation between the core and cladding fluid is 0.1, which can achieve ten to a hundred times in term of the refractive index modulation compared to the thermal effect and electro-optic effect. Consequently, the optical device with high refractive index modulation can be miniaturized in micron scale [5].

A hydrodynamic tunable switch is achieved by manipulating the flow rates of the three flow streams for the hydrodynamic focusing structure. By having differential

flow rates for each fluid streams, the width of the lower cladding fluid can be tuned in moving the reflective surface to different locations within the microchannel. This capability has achieved on-chip optical switching via the principle of TIR. As the hydrodynamic tunable optical switch can be integrated with other microfluidic functionalities, it holds promising potential to deliver optical switching functionality for lab-on-a-chip optical excitation and sensing applications. However, there are some remaining drawbacks of the hydrodynamic tunable switch, for instance the fluid's instability and limited life time. They will be addressed in chapter 3.

Chapter 3

Reflectivity based optofluidic switch based on cascading prisms

3.1 Conceptual design and optical principle for the optofluidic switch

The hydrodynamic tunable optical switch in chapter 2 has two limitations that led to the redesign of the optical tunable switch for further advancement [63]. Firstly, the optically reflective fluid-fluid interfaces of the hydrodynamic tunable optical switch in chapter 2 are inherently sensitive to the change of fluid pressure within the microchannels and the formation of micro sized bubbles. Secondly, the life time of the hydrodynamic tunable optical switch is limited as the formation of liquid-core liquid-cladding interfaces [21][63] require constant supply of calcium chloride solution and distilled water. Life time is defined as the length of time an optofluidic device can function before the supplying fluid is fully consumed. In the creation of pure fluid based optofluidic compartment, the formation of laminar flow or gradient refractive index (GRIN) fluid-fluid interfaces require constant supply of fluids. This has posed challenges in adaptation of optofluidic technology for mass-market product, which demands optical excitation and sensing applications that require optical functionality to be available for a long life time. In the redesign of the optofluidic tunable switch, the optical tunability found in hydrodynamic tunable optical switch within chapter 2 is retained. The new design is intended to counter the two practical drawbacks of the hydrodynamic tunable optical switch. In the new design depicted in Figure 3.1, two optofluidic cascading prisms are used to distribute light based on the principle of TIR and partial reflection.

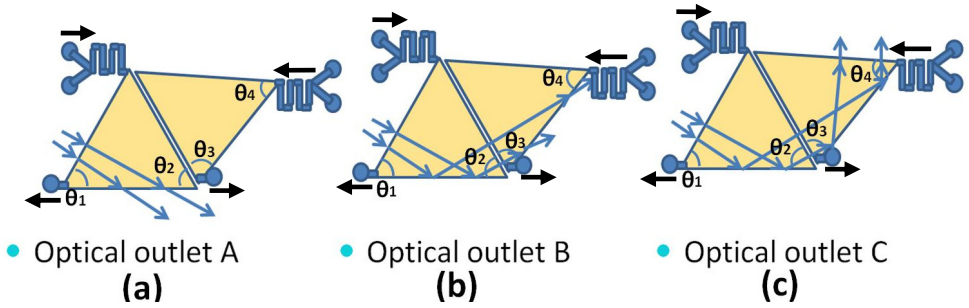

Figure 3.1 Optofluidic switch based on cascading prisms with three optical outlets

The light coupled into the optofluidic cascading prisms can be split or switched in micron scale according to different combinations of refractive index for each of the cascading prisms. The refractive index of the optofluidic cascading prisms can be changed separately in the range of 1.33 to 1.63 as two micromixers are attached to each of the optofluidic cascading prisms. The optofluidic switch based on cascading prisms does not rely on the continuous supply of fluids as there is no tunable fluid-fluid interface involved for the optical splitting or switching unlike the pure fluid based optofluidic devices [21][63]. The micromixers produce homogenous solution of benzothiazole (RI = 1.63) at different refractive indexes when the benzothiazole and isopropanol (RI=1.33) undergo micromixing at different combinations of flow rates. The micromixers need not continuously perform micromixing. Micromixing which requires consumption of fluids is only needed during the light switching or the change of the different proportions and intensities for the light splitting. When the optofluidic cascading prisms are filled with the benzothiazole solution with desired refractive index, the micromixer stops consuming fluids for micromixing until the next optical tuning. However, the optical functionality of the optofluidic cascading prism will not be affected because the fluid-solid interfaces are mechanically stable with its refractive index contrast between the PDMS and benzothiazole solution to achieve optical manipulations. Therefore, the fluid consumptions of Benzothiazole and isopropanol are reduced considerably due to

this tuning scheme. The new design of the optofluidic switch based on cascading prisms has a long life time. Furthermore, the mechanical stability of the optical interface improved considerably as the solid-liquid optical interfaces are not sensitive to the change of fluid pressure, formation of microbubble and particles. Even if the micro bubbles and particles reside in the cascading prisms' cavity, they will not disrupt the optical interfaces that are critical for maintaining the optical functionality. Furthermore, the microbubbles or particles can be flushed out of the cavity without disruption of the optical functionality. As a result, the elimination of the destabilization factors of the laminar flow caused by external factors or high Reynold number mixing will strengthen the optical stability of the optofluidic compartment. Compared to the optofluidic switch in chapter 2, the new design offers three optical outlets. The light can be either switched or distributed with same or different proportion among the three optical outlets, giving high versatility in manipulating light. The light switching capability is based on the principle of TIR, while the light splitting for distribution is based on principle of partial reflection. The new design derives the advantages of the solid based optical system, combined with the optical tunability of the fluid based optical system [21][63][66-68]. At the same time, the new design does not sacrifice the optical stability and the life time of the optical system.

The device working principle of the micro-light distribution system based on optofluidic cascading prisms is shown in Figure 3.1(a-c). The left and the right cascading prisms have different internal angles to allow the light path to remain approximately 90° at every coupling solid-liquid interfaces between the left and the right cascading prisms in order to reduce any optical attenuation or losses caused by refraction or TIR. The refractive indexes of the prisms and the PDMS are different.

The light pass from one prism to the next has an injection angle of 90°. The light does not undergo undesired refraction as the impinging angle is very small. In the left prism, θ_1 and θ_2 are 72° and 60°, respectively. In the right prism, θ_3 and θ_4 are 77° and 54°, respectively. The design of the placement for the input optical fiber is tilted 15° with respect to the horizontal axis of the left cascading prism. This horizontal axis is the first liquid-solid interface that the light can undergo the first TIR. The input laser hits the first liquid-solid interface with incidence angle which falls in the range of 65° to 80°. The refractive indexes of each cascading prisms can be tuned individually from 1.45 to 1.63 via the micromixing process of two miscible fluids with different refractive indexes. With different combinations of refractive indexes of the left and right cascading prisms, the light can be guided out of the cascading prisms via optical outlet A, B or C. In addition, there are many more combinations of refractive indexes that can realize different proportions of light distribution based on partial refraction. Figure 3.1(a) shows that the light passes through both of the two optical interfaces and exits from the optical outlet A. The refractive indexes of the left prism and the PDMS are the same which is 1.45. Figure 3.1(b) shows that the light is guided out of the cascading prisms via optical outlet B. This is achieved by tuning the refractive indexes of the left and right prisms to 1.63 and 1.45, respectively. When the refractive index of the left prisms is 1.63, the fluid-solid interface of the left prism gives the critical angle of 63°. The light coupled into the left prism with incidence angle of 65° to 80° undergoes TIR and the light is reflected on the first liquid-solid optical interface. The reflected light is coupled into the right cascading prism with refractive index of 1.45. The right cascading prisms has the same refractive index as the surrounding PDMS, hence the light is transmitted out of the right cascading prism via optical outlet B without

optical attenuation. Figures 3.1(c) shows the light is guided out of the cascading prisms via optical outlet C. The refractive index of both of the cascading prisms are 1.63, giving TIR at two individual fluid-solid optical surfaces which lead to the direction of the light being switched to optical outlet C. When the light within the optofluidic cascading prisms is switched from one optical outlet to the subsequent optical outlet, the light is distributed among two optical outlets. A portion of the incidence light is reflected while the remaining portion of the light is refracted. The fluid with higher refractive index within the cascading prism means higher reflectivity for the fluid-solid interface. The optical reflection constant of the fluid-solid optical interface is proportional to the amount of light reflected. When the light switches from optical outlet A to optical outlet B, the laser beam undergoes optical splitting based on partial refraction. The relationship between the reflection coefficient and the refractive index of the cascading prism for the fluid-solid interface is given by $R = \left(\frac{n_i \cos\theta_i - n_t \cos\theta_t}{n_i \cos\theta_i + n_t \cos\theta_t} \right)^2$ (Equation 3.1) [69] for both the s and p polarized laser beam, where n_i and n_t represent the refractive indexes of the incidence and transmittance medium respectively. θ_i and θ_t represent incidence and transmission angles respectively. From the relationship in the equation, lower reflection coefficient is due to higher refractive index of the transmittance medium n_t. On the contrary, higher reflection coefficient is due to higher refractive index of the incidence medium n_i. The input optical fiber is placed at 15° with respect to the horizontal direction of the liquid-solid interface within the left optofluidic cascading prism that allows the first TIR. The placement of the input optical fiber with a tilted angle would product the light with incidence angle between 65° and 80° which encompasses the range of incidence angle needed to

fulfil the criteria of TIR or partial refraction. V_{ben} represents the flow rate of the benzothiazole fluid inlet. V_{iso} represents the flow rate of the isopropanol fluid inlet. Two characteristics of benzothiazole make it suitable for PDMS based optofluidic compartment are its high refractive index of 1.63 and it does not swell PDMS. The distortion of the structure of the microchannels due to swelling will affect the bonding strength between the PDMS and glass slide. The flow rates of the benzothiazole (RI=1.63) fluidic inlet and isopropanol fluid (RI=1.33) inlet determine the resultant refractive index of the diluted benzothiazole solution. The combined flow rate of V_{ben} and V_{iso} is fixed at 60μl/min. By measuring the incidence and refraction angles of the incidence and refracted light beam transmitting from PDMS (RI=1.45) to dyed benzothiazole solution (RI=1.45-1.63), the refractive index of the transmittance medium within the cascading prism can be calculated according to Snell Law [88] $n_t = \frac{\sin\theta_i \times n_i}{\sin\theta_t}$ (Equation 3.2). n_i and n_t represent the refractive indices of PDMS and diluted benzothiazole solution, respectively.

3.2 Microchip fabrication and optical experiment setup

The microstructures on the four inches silicon wafer are made by single mask exposure in standard soft-lithography process. The negative mold for PDMS casting and peeling is produced according to the soft lithography processes illustrated in Chapter 1.3.2. Figure 3.2(a) shows the conjugated microchannels with 90° difference with respect to one another attach sequentially to form the micromixers. The width of each microchannel forming the micromixers is 90 μm. The smallest feature that the quartz mask can resolve is 3 μm. The finest structure in all the

microstructures with uniform height is 90 μm. The resolution of the quartz mask can produce microstructures with optically smooth sidewalls to reduce losses of light due to scattering. The width of the finest microstructure divided by the uniform height is approximately 1; hence the microstructures have good replication fidelity. Rhodamine B (Sigma- Aldrich) and Rhodamine 6G (Sigma- Aldrich) are mixed with methanol at 300 parts to 1 part weight ratio. Rhodamine B dyed methanol solution with excitation and emission wavelength of 540 and 625nm, is mixed with Benzothiazole and isopropanol at 100 parts to 1 part weight ratio for showing the lightpath within the optofluidic cascading prisms. The PDMS and its curing agent are mixed at 10 parts to 1 part weight ratio. The uncured PDMS is mixed with Rhodamine 6G dyed methanol solution with excitation and emission wavelengths of 526nm and 555nm at 100 parts to 1 part weight ratio for showing the lightpath within the PDMS. Two types of fluorescent dyes are utilized to separate the light transmitting inside and outside the optofluidic cascading prisms. After the dyed PDMS is cured at the temperature of 25°C for duration of 48 hours, the cured PDMS has a refractive index of 1.45 for the light with wavelength of 488nm. The PDMS slab undergoes oxygen plasma treatment (March plasma system PX-250, March Instruments Inc.) for a minute before bonding with transparent glass slide.

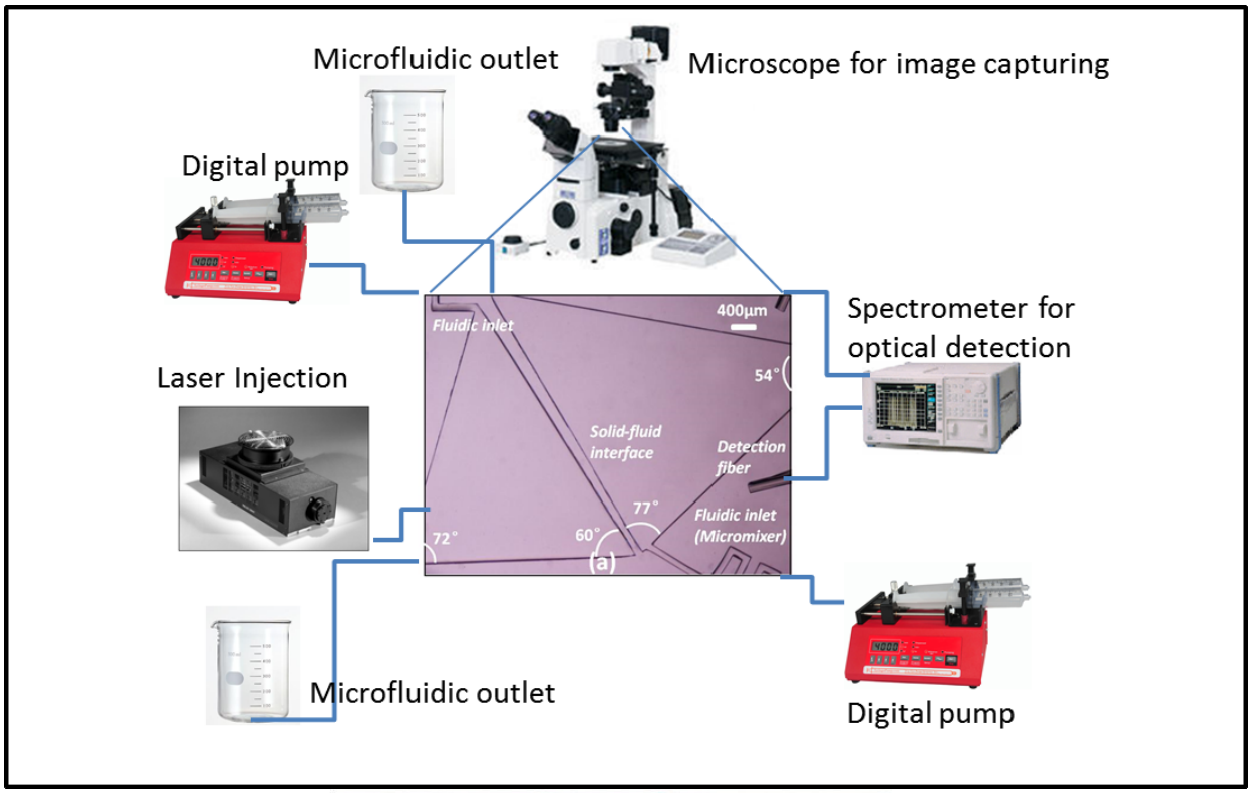

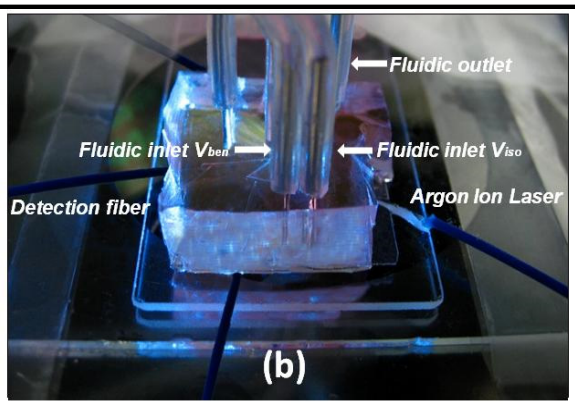

Figure 3.2 (a) Optofluidic circuit for the optical switch based on cascading prisms

(b) Microfluidic chip that is under optical experiment

The microchannels that are perpendicular to each other become the micromixers that achieve turbulence based micromixing in producing homogeneous mixture of the benzothiazole and isopropanol solutions. The refractive index of diluted benzothiazole solution is measured by Digital Hand-Held Refractometer (Reichert, AR200). The microchannels within the micromixers have a width and length of 95µm and 550µm, respectively. The subsequent microchannels connecting the aforementioned microchannels 90° with respect to each other have width and length

of 95μm and 280μm, respectively. The aforementioned combination of two microstructures connecting each other is repeated for seventeen times in forming the micromixer. This micromixer is connected to the optofluidic cascading prism to inject the homogenous solution into the prism with different refractive indexes. The benzothiazole or isopropanol solution exits from the prism via fluidic outlet depicted in Figure 3.2(b). One end of the tube (5212-B-90, EFD) is connected to the silicone tubing (06411-59, Cole Parmer) while the other end is connected to the PDMS chip. The other end of the silicone tubing is connected to a luer to carb connector (CX-012X, CONNEX). The luer to carb connector (CX-012X, CONNEX) is connected to a syringe driven by a digital pump for fluid injection purpose. These components all joined together in forming a fluid delivery system with controllable fluid flow rates for the benzothiazole and isopropanol solution. The microfluidic inlets supply fluids from the micromixers into the optofluidic cascading prisms. The minimum distance between the two cascading prisms is 100 μm. This is to ensure that the PDMS barrier between the two cascading prisms has sufficient bonding strength to adhere tightly with the glass slide. This would prevent the fluid from leaking from one prism to another, which will disrupt the optical functionality. The aspect ratio of the aforementioned PDMS barrier is 1.11. In the design of the microstructures, structures with high aspect ratios are avoided to prevent low adhering strength between the PDMS and the glass slide substrate. With the design of the microstructures with low aspect ratio, the bonding process between the PDMS and the glass slide substrate will produce high bonding strength. Higher adhering strength between the PDMS and the glass slide substrate is important to prevent the fluid within the optofluidic cascading prisms from leaking in the microchip. The height of the microchannel measured by the profilometer is

90 μm.

The laser light is coupled into the microchip for optical light switching and splitting with the integration of optical fiber (Silicon Lightwave Technology, outer diameter =125 μm, core diameter = 62.5 μm, and numerical aperture NA = 0.22) with the microchannels. The tip of the optical fiber is rendered a flat surface by cutting it with a high precision cleaver (CT-30A, Fujikura). The optical fiber is then positioned 80 μm from the left optofluidic prism with an angle of 75° with respect to the first horizontal reflective surface within the left prism. The angled position for the placement of the optical fiber is measured by using protractor during the design of the microstructure in L-edit layout design software before the device fabrication. Due to the flat surface for the tip of the optical fiber, there is no space left between the optical fiber and the sidewall of the PDMS optical fiber insertion slot. Consequently, the optical scattering is minimized at the tip of the optical fiber to reduce optical losses during the optical coupling. The optical fiber is connected to 488nm argon ion laser light source (532-AP-A01, Melles Griot) with intensity of 150mW. Each of the optofluidic prisms is supplied with fluid via micromixer. With different refractive indexes of the left and right optofluidic cascading prisms, the distribution of light power to different optical outlets can be varied by controlling the flow speeds of the two microfluidic inlets carrying benzothiazole and isopropanol solutions into the micromixer, producing the homogenous mixture of diluted benzothiazole solutions. Tunable distribution of light power is achieved with the principle of TIR and partial refraction. The benzothiazole and isopropanol have a refractive index of 1.63 and 1.33, respectively. Both fluids are mixed with Rhodamine B dye solution at 150 parts to 1 part weight ratio. The lightpath in the fluid and PDMS are visible as the dye within the fluid and PDMS is excited by the

488nm Argon Ion light source. The lightpath shows the light diverges more as it undergoes multiple TIR causing the reduction in the optical power. The output light is coupled to a multimode optical fiber before measured by the spectrometer. The spectrometer (HR4000, Ocean Optics Inc.) is used to detect the optical power from three optical outlets as shown in Figure 3.2(b). The experimental pictures of the optofluidic cascading prisms are taken by a charge-coupled digital camera (DP70, Olympus) attached to the inverted microscope (TE2000-E, Nikon). The focus of the microscope is fixed at the middle height of the microchannels to produce the sharpest image quality. For each beam intensity corresponding to different refractive indexes for both the left and right prisms, twenty times of repeated measurements are conducted. The repeated measurements reduce the measurement errors caused by the non-uniform light output via the multimode fiber. The average value derived from these twenty measurements is taken as the average beam intensity. During each set of measurements, the optical fiber remains stationary to prevent the measurement discrepancies of the optical intensity.

3.3 Results and analysis for the optofluidic switching experiment

When the optofluidic prism on the left is filled with diluted benzothiazole with refractive index of 1.45, the laser beam passes through the solid-fluid interface without optical attenuation because the refractive index of the optofluidic prism is the same as the PDMS as shown in Figure 3.3(a). When the laser beam exits the left optofluidic prism, the optical power decreased by 6% with respect to the original optical power due to the diverging of the laser beam. When the left optofluidic prism is filled with benzothiazole solution with refractive index of 1.63, the first reflective surface within the left optofluidic prism has the TIR angle of 63°. The

laser beam impinges on the first reflective surface with incidence angle from 65° to 80°. Consequently, the laser beam is fully reflected at the optical interface and the reflected laser beam is coupled into the right optofluidic prism. The right optofluidic prism is injected with benzothiazole solution with refractive index of 1.45, hence the laser beam penetrates through and exits the optofluidic right prism without optical attenuation via optical outlet B. The optical power detected at the

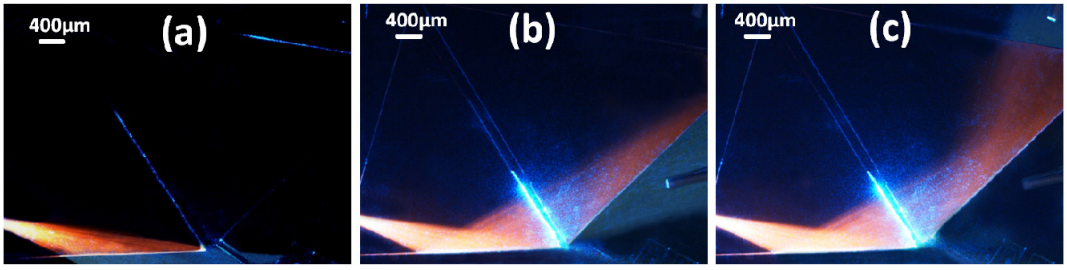

Figure 3.3 (a-c) Optical switching experiment pictures via three optical oputlets

This is because of the fact that the laser beam width at optical outlet B is 96% wider than the laser beam width at the optical outlet A of left optofluidic prism.

Both of the optofluidic cascading prisms is filled with benzothiazole solution with refractive index of 1.63, the TIR angle for both the fluid-solid reflective surfaces is 63°. The incidence angle for the laser beam impinging on the second solid-fluid reflective surface is between 63° and 72°, fulfilling the criteria for the laser beam to undergo TIR at the second fluid-solid reflective surface. The laser beam is fully reflected twice on the two fluid-solid reflective surfaces within the optofluidic cascading prisms and exits from the optical outlet C. Comparing the optical power detected at optical outlet C and the case where the laser beam is guided out of the microchip via optical outlet B, the optical power at optical outlet C is 37% less than the optical power detected at optical outlet B. The divergence of the laser beam leads to the reduction of optical power after the light undergoes multiple TIR. The beam width at the optical outlet C is 81% wider than the incidence beam width

within the right optofluidic prism. In Figure 3.3(a), the optical power is reduced by 6% due to (i) the adsorption of the benzothiazole fluid, (ii) optical scattering at two solid-fluid interfaces of the left optofluidic prism and (iii) widening of the laser beam width. The reduction of optical power caused by the adsorption of benzothiazole fluid and optical scattering only represents a small and insignificant portion of the optical loss compared to the total optical power detected at optical outlet A. John et al. [70] shows that the benzothiazole fluid will absorb light with wavelength of 220 to 290nm while the absorption of light at 488nm is insignificant. The PDMS sidewalls are optically smooth and transparent, hence the solid-fluid interfaces of the optofluidic cascading prism and the PDMS barrier do not attenuate light and cause minimal change to the optical power when the laser beam penetrate through perpendicular to the optical surfaces. The light intensity detected at the optical outlet C is 15.54% of the original light intensity as the light undergoes two TIR. The major cause for the decrease of the optical power is the divergence of the laser beam. The light switching capability of the optofluidic cascading prisms to divert the laser beam into any of the three optical outlets is demonstrated.

3.4 Optical reflectivity analysis based on partial refraction

Besides optical switching, the optofluidic cascading prisms also provide flexibility of a micron scale light distribution system based on the principle of partial refraction. As there are two reflective surfaces in each of the optofluidic cascading prisms, the micro-light distribution system provides distribution of single laser beam into three separate beams at desired proportions of optical power. The single laser beam undergoes beam splitting for two times and becomes three individual light beams. When the refractive indexes of both the optofluidic cascading prisms is

tuned at the same value ranging from 1.47 to 1.61 for optical detection at optical outlet B, the optical splitting is observed for the calculation of the value of optical reflection constant. The optical power detected at the optical outlet A, when the left optofluidic prism is at refractive index of 1.45, is recorded. After that, the refractive indexes of both of the optofluidic cascading prisms is changed to 1.53 for the measurement of optical power at optical outlet B. From the experimental photos in the Figure 3.3(b), partial refraction is realized when both of the optofluidic cascading prisms is filled with diluted benzothiazole solution with refractive index of 1.53. The value of optical reflection constant is calculated by dividing 'the different optical power detected at optical outlet B' by 'the optical power detected at optical outlet A' via optical fiber when there is no mismatch of refractive index between the PDMS and the left optofluidic prism, whereby the left optofluidic prism let the laser beam passes through without refraction or reflection. The optical power detected at optical outlet B increases in proportion to the increase of refractive indexes of both of the cascading prisms. Consequently, the value of optical reflection constant increases as the refractive indexes of both the optofluidic cascading prisms increases.

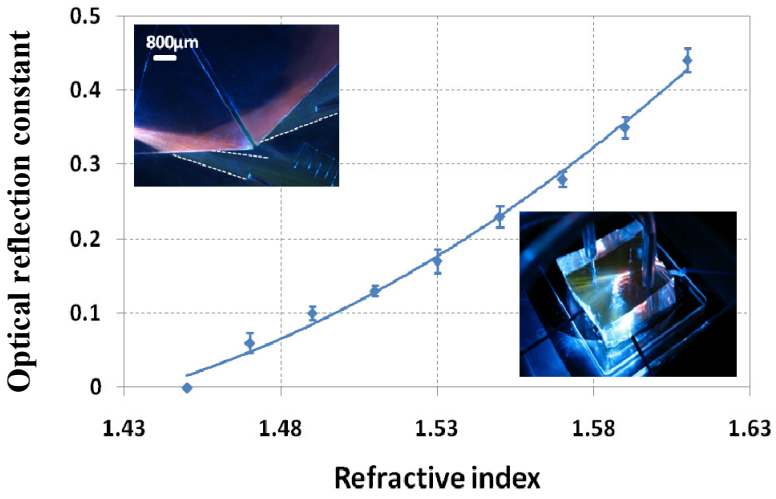

Figure 3.4 Optical reflection constant manipulations by altering the refractive indexes for both cascading prisms

The value of optical reflection constant is always lower than 1 because the laser beam undergoes partial refraction and the divergence of the laser beam. Figure 3.4 gives the relationship between the optical reflection constant and the refractive indexes of the optofluidic cascading prisms ranges from 1.47 to 1.61. The highest standard deviation for the optical reflection constant at different refractive indexes is 0.307786 for the sample size of 20. The signal to noise ratio for the measurement of optical intensity is 300:1. The higher the value of the optical reflection constant in Figure 3.4 means more light is reflected from the first reflective surface within the left optofluidic prism. This is achieved by increasing the refractive index of the fluid injected into the left optofluidic prism. Besides tuning the refractive indexes of both the cascading prisms to the same value, there are numerous combinations of refractive index for the left and right optofluidic prisms, which enable variable optical power distribution from a single light source to multiple optical outlets.

3.5 Refractive index generation and analysis based on micromixing

The homogenous benzothiazole solution is produced by the micromixer with microchannels that are perpendicular to each other. Different flow speeds from the isopropanol fluid inlet and benzothiazole fluid inlet produce benzothiazole solution at different refractive indexes. Figure 3.5 shows how the variation of the fluid flow speeds of isopropanol and benzothiazole affect the refractive indexes of the homogenous solutions produced. The total flow speed of the two fluidic inlets is 60μl/min. The micromixing speeds by two microfluidic inlets for each refractive index are tested twenty times to obtain the average refractive indexes. The refractive indexes of the benzothiazole solutions are measured by refractometer. The highest standard deviation for the refractive index measurement based on

micromixing at different flow rates is 0.004069 for sample size of 20. The measurement error for the refractive index sensing based on the highest resolution of the refractometer (Reichert, AR200) is 0.001. The measurement error the flow rate controlled by the digital pump is 0.1 µl/min.

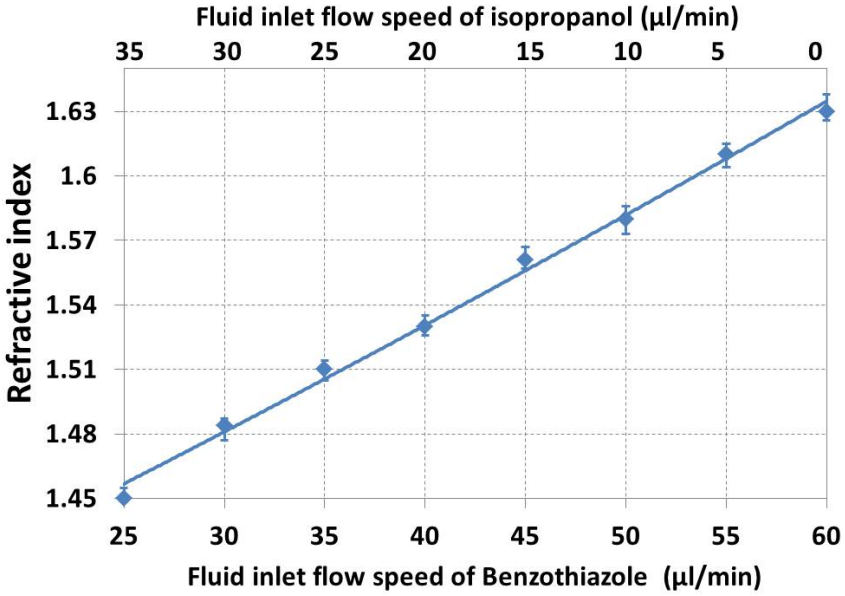

Figure 3.5 Tunability of the refractive index based on micromixing at different flow speeds

The speed of laser beam to switch from optical outlet A to optical outlet C depends on the time taken to replace the fluid with refractive index of 1.45 within the optofluidic cascading prism to fluid with refractive index of 1.63. This process takes about two seconds. The time taken for the fluid within the prism with refractive index of 1.63 to be tuned down to 1.45 takes seven seconds which is much longer than the tuning of the refractive index from 1.45 to 1.63 because backpressure is generated when the high-viscosity benzothiazole solution is flushed out of the microchip which is replaced by the low-viscosity diluted benzothiazole solution. The time taken for micromixing to be completed in producing the homogenous diluted benzothiazole solution with a bulk refractive index is ten seconds. The speed of completing the micromixing process is not constant. It

depends on the initial and the resultant viscosity of the benzothiazole solution. Higher initial viscosity of the benzothiazole solution increases the micromixing time as more time is needed for the lower viscosity benzothiazole solution to push the higher viscosity benzothiazole solution out of the microchannels. When higher viscosity of the benzothiazole solution is used to push the lower viscosity benzothiazole solution after micromixing, then the time taken for the micromixing is shorter. The laser beam scattering can be eliminated by switching the laser beam off temporarily. The laser beam can be turned on again once the micromixing process is completed, filling the optofluidic cascading prisms with homogenous solution of the same refractive index. When the total flow rate of the benzothiazole and isopropanol is increased, the micromixing process will be hastened. This would increase the speed of optical tuning as the time taken for the refractive index to change from one to another is shortened. Note that many bio-excitation and sensing applications like fluorescence microscopy and bioassays do not demand fast optical tuning [22]. For the purpose of direct comparison, the volume of fluid needed for the optofluidic compartment to perform three optical tunings in eight hours is calculated for the optofluidic switch based on cascading prism and optofluidic compartment that make use of liquid-core liquid-cladding fluid interface [66]. The optofluidic switch based on cascading prisms is a static device rather than a dynamic device [66].

3.6 Recommendation and conclusion

The incorporation of solid-fluid interface represents a new class of optical devices by merging the advantages of optical system with pure solid-solid or fluid-fluid interfaces into a micro-light distribution system. The fabricated PDMS chip has a

uniform refractive index unlike crystalline or birefringent material that can functions as an optically active polarization filter to alter the polarization of the light. Consequently, the optofluidic cascading prisms do not change the polarization of the laser beam even if it undergoes one or two TIR. When the optofluidic cascading prisms are filled with benzothiazole with refractive index of 1.63 and the PDMS with refractive index of 1.45, the Brewster's angle is calculated as 48.34°. Since the incidence angle for the first reflective surface within the left optofluidic prism is between 65° and 80°, the polarization of the incidence light will not change. PDMS possess excellent optical transparency to minimize the optical losses while the laser beam is transmitted within the PDMS medium.

The width of the beam gradually increases as the laser beam propagates within the optofluidic cascading prisms. The optical light path's divergence is in proportion to the distance of propagation. The micro-light distribution system based on optofluidic cascading prisms offers capability to distribute light in micron scale. It is achieved through optical splitting at two fluid-solid surfaces with tunable reflectivity. The functionality of the optofluidic cascading prisms cannot be replicated in the optical system with solid-solid interfaces as it is specially catered to lab-on-a-chip applications. In addition, the micro-light distribution system can be integrated into the PDMS based microfluidic circuits with one layer standard soft lithography process. The fast and simple fabrication process will hasten the speed of integration of the micro-light distribution system with optical excitation and sensing applications. The cavity of the left and right optofluidic prism needs 0.46 μl and 0.77 μl of solutions to achieve complete filling, respectively. The time taken for the optical switching can be further shortened by increasing the total flow rate from the two fluidic inlets. However, most bio-excitation and sensing applications do not

need short optical switching duration [22]. When the optofluidic cascading prisms are filled with benzothiazole solution at refractive index of 1.63, the mismatch of refractive index between the optofluidic cascading prisms and the PDMS is 0.19. This amount of mismatch in refractive index is about twenty to two hundred times the refractive index's mismatch of the optical system based on thermal and electro-optic principle. Higher mismatch of refractive index is favored because it enables the scaling down of the size of the optical system to micron scale. The micro-light distribution system can be furthered scaled down to tens of micron. The micro-light distribution system has the possibility to be developed into an optical evanescent wave sensor if the evanescent wave can be detected at the optical surface which the TIR occurs. The optical evanescent wave sensor detects different optical intensities and correlates them with fluid concentrations or refractive indexes of fluids. The applications of the evanescence sensor can be extended into light intensity sensing utilizing light source with multiple wavelengths. A micro-light distribution system via optofluidic cascading prisms with tunable reflectivity is investigated in this chapter. The tuning of different optical reflectivity is achieved by manipulating the flow rates of two microfluidic inlets injecting into two separate micromixers. By changing the optical reflectivity of the fluid-solid surfaces, TIR and partial reflection can be achieved to realize optical switching and splitting. By varying the differential flow rates between the two microfluidic inlets carrying benzothiazole and isopropanol solutions, different refractive indexes of the cascading prisms can be tuned individually. Consequently, different proportions of light distribution can be tuned. The planar micro-light distribution system provides high versatility in varying the design of MOFS. If more sets of cascading prisms are combined, a multi-degree-of-freedom light manipulation system can be realized. The micro-light

distribution system via optofluidic cascading prisms represents a promising optofluidic compartment to realize an on-chip planar light distribution catering to high power laser light distribution. This optofluidic compartment can be integrated in many lab-on-a-chip optical excitation and sensing applications. In this chapter, we have solved some of the drawbacks of the optofluidic switch in chapter 2 and extended the switching capability. In the process, the optical partial refraction phenomenon is studied which leads to chapter 4 of studying the optical partial refraction phenomenon in an optofluidic refractive index sensor.

Chapter 4

An optofluidic refractive index sensor based on partial refraction

4.1 Concept and optical principle for the optofluidic refractive index sensor

In the previous chapter, the optical partial refraction has been observed during the optical switching processes, which leads to the development of an optofluidic refractive index sensor in this chapter. The current technology implemented for refractive index sensing usually employs more complicated fabrication processes. Consequently, it cannot be integrated in a polydimethylsiloxane (PDMS) chip with single layer microchannels. Traditional sensing technique involves the use of fluorescence emission from the fluid analyte produced by optical excitation. Based on the intensity and characteristic of the fluorescence emission, the changes of the refractive index can be detected. The earlier refractive index measurement system utilizes the surface plasma wave propagation along a gold layer surrounded by two dielectrics material as an integrated optical waveguide structure for optical sensing. The limitation of this method is that it requires large sensing area which increases the consumption of fluidic analyte. Consequently, a method based on localized surface-plasmon-resonance [72] is proposed using sensor probe formed at the end of a multimode fiber. The gold nanoparticles are immobilized on the fiber probe for fluidic analyte refractive index sensing. This sensing technique requires less amount of fluidic analyte compared to the conventional surface-plasmon-resonance sensor.

Among these sensing techniques, evanescent wave, fluorescence, and surface-plasmon-resonance are compatible with microfluidic devices. The aim is to implement refractive index sensing in planar PDMS device by utilizing the optical principle of partial refraction at the fluid-solid interface [73]. This refractive sensing technique only needs to consume less than one hundred microliters of the fluid for analysis. The refractive sensing technique based on partial refraction provides fast sensing capability for noncontact and label free sensing specimen. The planar microfluidic channels have low height to width ratio which yields sufficient bonding strength to prevent fluid leakage. The refractive index can be detected by measuring the refraction angle or the intensity of the refracted light. The optical reflection constant can also be calculated subsequently. The microchip is made by employing the standard soft lithography process which only involves a single layer mask exposure and wafer development.

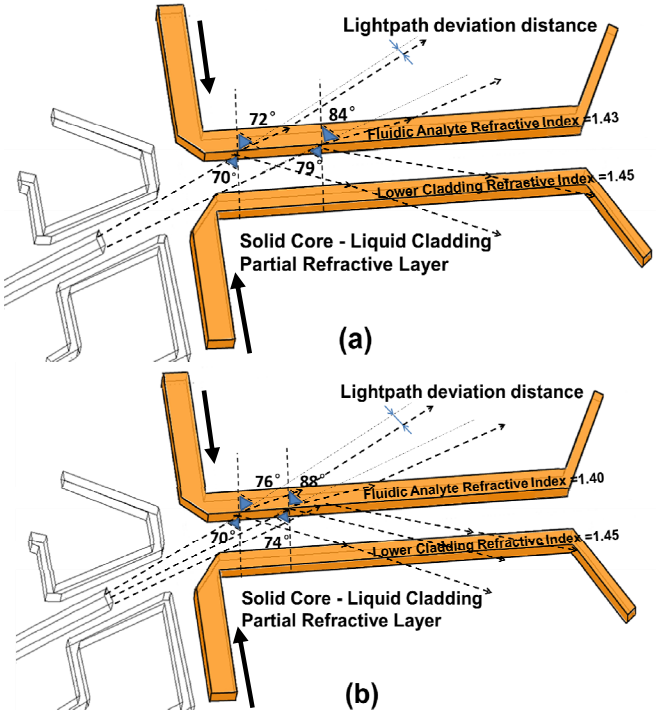

Figure 4.1 (a-b) Schematics of the optofluidic refractive index sensor correspond to the fluidic analyte refractive index at 1.43 and 1.40

The optical partial refraction is the mechanism the optofluidic refractive index employs to achieve refractive index sensing. The sensing structure is made up of a solid core of PDMS with refractive index of 1.45 and two liquid cladding. The refractive index of the liquid cladding is measured and correlated by the optical reflection constant and refraction angle. The measuring range of the refractive index of the fluid analyte is between 1.37 and 1.45. The increment of the fluid analyte concentration will result in a higher refractive index of the fluid to be analyzed. The microchannel of the lower cladding is filled with fluid with refractive index of 1.45. The purpose of the lower cladding channel is to ensure that the light is not refracted by the optical interfaces when the refractive index of the fluid is 1.45, ensuring that the optical light path is not severely affected by the optical interfaces. The refractive index of the PDMS solid core is fixed at 1.45. This configuration leads to the TIR angle of 80.4°. This optical experiment picture is depicted in Figure 4.1(a) which shows the diverging laser beam having incidence angle ranges from 70° to 79°. The incidence light with incidence angle of 79° is fairly close to the TIR angle and the refraction angle for the incidence light of 79° is 84.5°. When the refractive index of the fluid within the upper cladding is tuned at 1.40, the TIR angle at the solid-fluid interface is determined to be 74.9° with the refractive index of the solid core remains at 1.45. The light impinges on the solid-fluid interface with incidence angle which is 1°-5° less than the TIR angle of 74.9° would undergo partial refraction. The percentage of the light reflected increases when the difference between the incidence angle and the TIR angle is decreased. When the incidence angle of the light exceeds the TIR angle, the laser beam would be totally reflected at the solid-fluid interface. Figure 4.1(b) shows that the light impinging on the solid-fluid interface at 74° are approximately the final ray of light that is partially refracted

before TIR occurs. The refraction angle determined from Snell's law for this particular ray of light with incidence angle of 74° is 84.6° while TIR angle is calculated to be 74.9°. The light beam that undergoes reflection consists of a portion of light that TIR. The measurement of the refraction angle and the divergence distance of the laser beam that impinges on the solid-fluid interface at 70° can be attributed to the fluid residing in the upper cladding microchannel with different refractive indexes. Divergence distance is defined as the distance of the diverged light transmitted through the microchannel with different refractive index to the same ray of light if transmitted in the medium with same refractive index. Consequently, this detection scheme we used can achieve refractive index sensing. Larger angle of refraction leads to longer divergence distance. Hence, the angle of refraction is proportional to the divergence distance. The value of optical reflection constant is obtained by dividing 'the average light intensity of the reflected laser beam transmitting within the solid core' by 'the average light intensity of the laser beam impinging on the solid-fluid interface'. The optical intensity of the light is measured by the pixel intensity captured by the CCD of the microscope. As the refractive index of the fluid in the upper cladding microchannel is tuned from 1.37 to 1.45, the average optical intensity for the laser beam that undergoes reflection decreases. By measuring the average optical intensity of the incoming laser beam and the average optical intensity of the reflected light beam, optical reflection constant can be calculated and correlated to the sensing refractive index of the fluid. The factors that affect the optical refraction angle include the two refractive indexes of the light propagating mediums and the angle of incidence. Their relationship [19] is described as:

$$n_i \sin\theta_i = n_t \sin\theta_t \quad \text{(Equation 4.1)}$$

where θ_i and θ_t represent the angle which the light impinges on the solid-fluid interface and the refraction angle after the light transmits through into the different medium. The factors that affect the optical reflection constant are (i) two refractive indexes of the light propagating mediums, (ii) the cross-sectional area and (iii) optical intensity of the light that impinges on the solid-fluid interface in the transmitting medium, (iv) the cross-sectional area and (v) optical intensity of the light that is refracted from the solid-fluid interface and (vi) the optical intensity of the reflected light. The relationship between these factors and the reflection coefficient is given by:

$$R = \left(\frac{n_i \cos\theta_i - n_t \cos\theta_t}{n_i \cos\theta_i + n_t \cos\theta_t} \right)^2 \quad \text{(Equation 4.2)}$$

for the s-polarized laser beam, where n_i and n_t represent the refractive indexes of the incidence and transmittance medium respectively. θ_i and θ_t represent incidence and transmission angles respectively. From the relationship in the equation, lower reflection coefficient is due to higher refractive index of the transmittance medium n_t . On the other hand, higher reflection coefficient is due to higher refractive index of the incidence medium n_i . When the refractive index of the fluid within the upper cladding microchannel n_t increases, the TIR angle increases, leading to reduced optical reflection constant as less amount of light is fully reflected at the solid-fluid interface.

4.2 Microchip fabrication and optical experiment setup

The fabrication of the microchip for the optical experiment is prepared by conventional soft lithography process. 0.01 $gmol^{-1}$ PBS solution (Sigma Aldrich) is

used to mix with Chromeon 482 fluorescent dye (Sigma Aldrich) at 500 parts to 1 part in weight ratio to produce the dyed solution. The PDMS elastomer is mixed with its curing agent (Sylgard 184 Silicone Elastomer Kit) at 10 parts to 1 part in weight ratio. The bubbles generated in the mixing process are eliminated in the degassing process. The aforementioned dyed solution and the PDMS are then mixed at 1 part to 100 parts in weight ratio. The mixing of the fluorescence dye and the PDMS is to make the light path visible as the Chromeon 482 fluorescent dye can be excited at 482nm and would emit light with wavelength of 507nm.

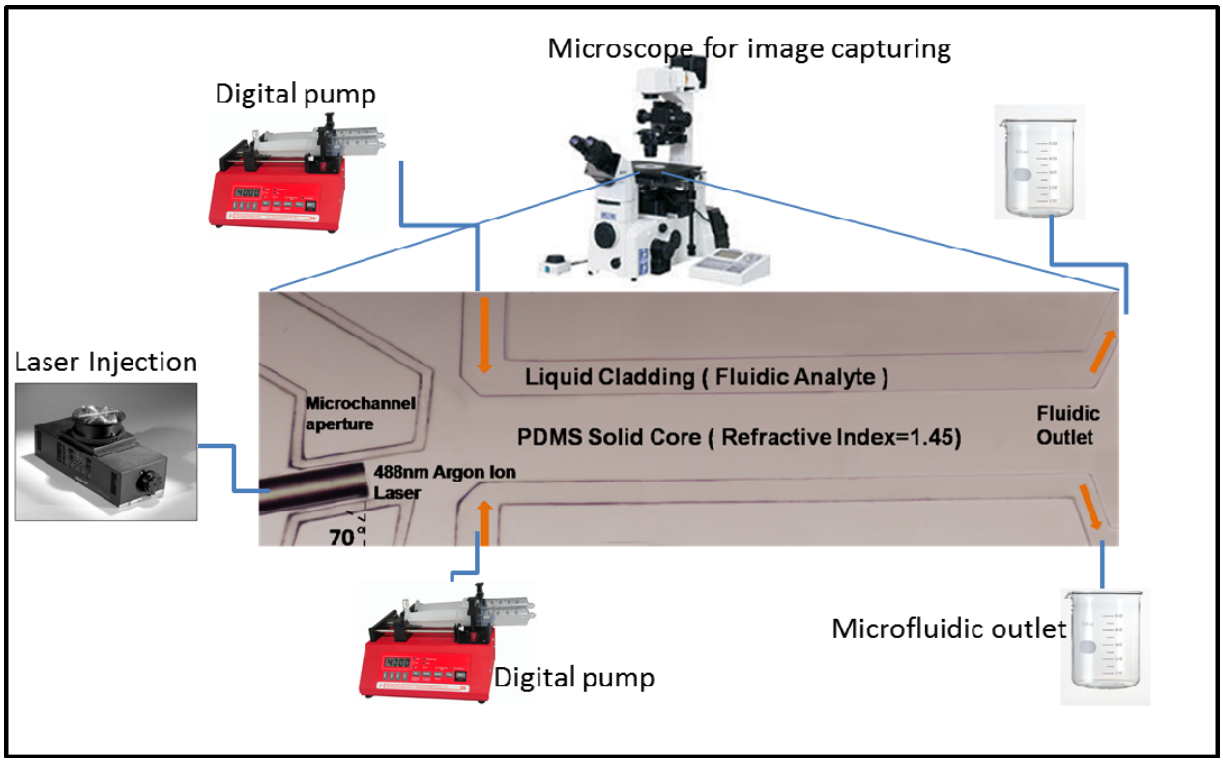

Figure 4.2 Optofluidic circuit for refractive index sensing based on partial refraction

Figure 4.2 depicts the fabricated microchip from the standard PDMS pouring and peeling process. The microstructure on the wafer is imprinted onto the PDMS and become the microchannels. The curing of the dyed PDMS takes 48 hours at temperature of 25°C. Under the light with wavelength of 488nm, the refractive index of the cured PDMS is 1.45. The preparation of calcium chloride solution is done by dissolving the calcium chloride powder in the distilled water. The

measurement of refractive index of calcium chloride solution at 1.45 is done by Digital Hand-Held Refractometer (Reichert, AR200). The Argon Ion laser light source (532-AP-A01, Melles Griot) at 488nm is injected into the microchip when the upper cladding microchannel is filled with the calcium chloride solution with refractive index of 1.45. There is no mismatch between the refractive index of the microchannel and the surrounding PDMS. Consequently, all the light passes through the upper cladding microchannel without reflection. Hence it is tested experimentally that the PDMS curing for 48 hours at 25°C yields the optical transmission medium with refractive index of 1.45.

The surface of the PDMS chip with the microchannel and the glass slide with smooth surface undergoes plasma surface treatment (March plasma system PX-250, March Instruments Inc.) for one minute before bonding together in becoming a functional microchip. The widths of the PDMS solid core, the upper cladding microchannel and lower cladding microchannel are 295 μm, 120 μm and 80 μm, respectively. The upper and lower cladding microchannels have length of 2000 μm with microfluidic inlets and another outlet with microchannel height of 80 μm, as measured by the profilometer. The microchannel is fabricated together with the fiber insertion slot. To render the surface on the tip of the optical fiber smooth and flat, the optical fiber is cut by high precision cleaver (CT-30A, Fujikura). This step is to ensure that there is no cavity or space when the optical fiber is inserted into the fiber insertion slot to minimize light scattering. The fiber insertion slot is filled with isopropanol to reduce the friction during the optical fiber insertion. The fiber insertion slot having width of 125 μm is inserted with a multi-mode optical fiber (Silicon Lightwave Technology) with outer and core diameter of 125 μm and 62.5 μm, respectively. This optical fiber having the numerical aperture of 0.22 is aligned

on the lower left corner with 70° with respect to the vertical axis. The aperture constructed surrounding the optical fiber would be filled with black ink to block the diverging laser beam from impinging on the surrounding microchannels, which will causes light scattering and multiple optical reflections. The optical fiber is connected to the light source of Argon Ion laser at the power of 150mW. The calcium chloride solution with refractive index ranges from 1.37 to 1.45 is mixed with Chromeon 482 dyed solution at 200:1 weight ratio. The dyed calcium chloride solution is injected into the upper cladding microchannel. The lower cladding microchannel is filled with calcium chloride solution at refractive index of 1.45 without fluorescent dye in the solution. The microscope picture of the optofluidic device is taken by the charge-coupled digital camera (DS-Fi1, Nikon) connected to the inverted microscope (Nikon Eclipse TS100). The optical reflection constant obtained from the incidence and reflected light intensity with or without partial refraction is feasible in correlating to the fluid analyte refractive index if the digital camera sensor is not over exposed or saturated. The light intensity for the fluorescence emission is proportional to the light intensity for the fluorescence excitation. The experimental picture captured is analyzed by software (MATLAB 7.0 R14) to obtain the average pixel intensity at (i) the area before the light impinges on the solid-fluid interface and (ii) the area which consists of the reflected light after the partial refraction at the solid-fluid interface. The average pixel intensity for the region before and after the partial refraction is used to calculate the optical reflection constant. Within the optical incidence and reflection regions, the pixels intensity having the same horizontal height as the overlapping point is analyzed to obtain the average pixel intensity. The image is inputted into (MATLAB 7.0 R14) for converting the experimental photos into pixel intensities

representing the optical intensity of each pixels. The pixel intensity values on the dotted line in the detection regions are averaged for the incidence and reflectance regions. The averaged value of the pixel intensity on the dotted line in reflectance region divided by the averaged pixel intensity at the dotted line in the incidence region gives the optical reflection constant. This analysis and averaging of pixel intensity is conducted three times for any particular refractive index. The width of the upper cladding microchannel is 1.5 times the height of the same microchannel. During the experiment, the focal plane is focused on the central height of the microchannel to obtain clear experimental pictures.

4.3 Optofluidic refractive index sensing results and analysis

When the upper cladding microchannel is injected with calcium chloride solution at refractive index of 1.40, the refraction angle measured experimentally from the lightpath is 76°. The refraction angle predicted from the theoretical formula of Snell's law is 0.7° more than the experimental value. The analysis shows that the intensity of the light is reduced by 27% leading to the optical reflection constant of 0.73 when the upper cladding microchannel is filled with calcium chloride solution at refractive index of 1.40. The incidence light is deviated by 51 μm after the laser beam undergoes partial refraction as shown in Figure 4.3(a). When the calcium chloride solution at refractive index of 1.43 is injected into the upper cladding microchannel, the experimental refraction angle is measured at 72°, while the theoretical calculation of refraction angle based on Snell's law is 72.3° as shown in Figure 4.3(b). The measurement of the refraction angle is conducted by magnifying the experiment photos by five times and measuring the refraction angle with protractor.

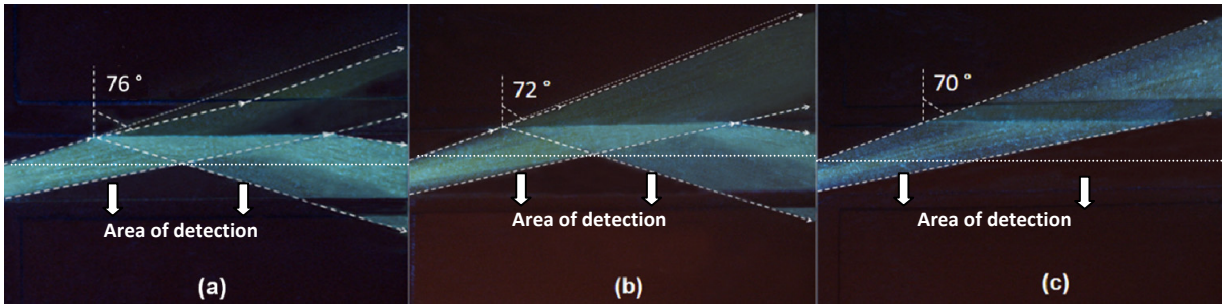

Figure 4.3 Optical experimental pictures of partial refraction when the refractive indexes of the upper cladding are tuned at (a) 1.40, (b) 1.43, and (c) 1.45 respectively

The laser beam is deviated by 20 μm, which is 31 μm less than the lightpath deviation distance when the refractive index of the upper cladding is 1.40. When the fluid within the upper cladding microchannel is 1.43, the optical reflection constant is approximately 0.55. This implies an optical loss of 45% compared to the incidence light beam. Figure 4.3(c) illustrated the lightpath where the fluid with refractive index of 1.45 is injected into the upper cladding microchannel. The laser beam is directly transmitted through the microchannel without optical attenuation. There is no refractive index mismatch between the microchannel and the PDMS at refractive index of 1.45. There is no optical refraction or optical reflection observed in Figure 4.3(c) when the light passes through the optical interfaces. Consequently, the value for the optical reflection constant is zero when the upper cladding microchannel is filled with calcium chloride solution with refractive index of 1.45. The optical power loss is due to the diverging of the laser beam rather than the partial refraction. The measurement is done by averaging the pixel intensity of the area of detections depicted by the dotted line in Figure 4.3.

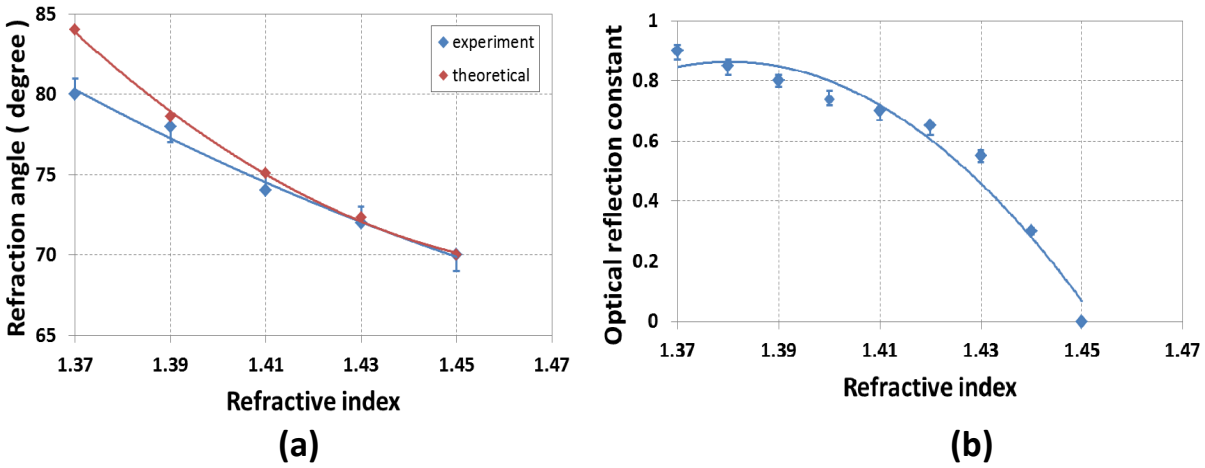

Figure 4.4 (a) The change of refraction angle with respect to different refractive indexes (b) Different optical reflection constant correspond to different fluidic analyte's refractive index

Figure 4.4(a) shows the relationship between the refractive index of the fluid analyte and the refraction angle for incidence angle of 70° measured at different refractive indexes. The sensing range of the refractive index depicted in Figure 4.4(a) is between 1.37 and 1.45 with the correlation of refraction angle that gradually decreases from 80° to 70° as the refractive index gradually increases from 1.37 to 1.45. The measurement error of the refraction angle is ±1°. The maximum discrepancy between the highest and lowest refraction angle measured using the protractor is 1°. Two curves plotted using curve fitting by second order polynomial are shown in Figure 4.4(a), which represent the theoretical and experimental data. The two curves of experimental and theoretical calculation for the refraction angle show that they obtain close agreement with each other. When the upper cladding microchannel is injected with fluid at refractive index of 1.37, the laser beam undergoes TIR when the angle of incidence exceeds the TIR angle of 70°. Equation 4.1 depicts the inverse proportional relationship between refraction angle and the refractive index n_t of the medium after the light transmitted through the solid-fluid interface. The inverse proportional relationship between the refractive index of the

fluid analyte and the optical reflection constant is given by Figure 4.4(b). The curve fitting for data points within the Figure 4.4(b) is based on second order polynomial. Figure 4.4(b) shows that when the refractive index of the fluid analyte increases from 1.37 to 1.45, the optical reflection constant decreases from 0.9 to 0. The largest measuring range for the optical reflection constants at refractive index of 1.37 is 0.87 to 0.92. The aforementioned Equation 4.2 shows that optical reflection constant is inversely proportional to the refractive index of the medium after the light passes through the solid-fluid interface. The relationships between the refractive index of the transmitting medium, optical refraction angle and optical reflection constant modeled by Equation (4.1) and Equation (4.2) correlate well between the theoretical prediction and the experimental data. The sensing resolutions of the optofluidic refractive index sensors based on partial refraction are 0.02 and 0.01 for the sensing mechanism based on refraction angle and optical reflection constant, respectively. In the experiment, the change of refractive index of 0.01 of the calcium chloride solution measured by Digital Hand-Held Refractometer (Reichert, AR200) will induce detectable change in optical reflection constant. The refractive index resolution of the Digital Hand-Held Refractometer (Reichert, AR200) is down to 0.0001. Future improvement can be made by preparing calcium chloride solution with refractive index difference of 0.0001 and conducting the experiment to measure the optical reflection constant. The change of refraction angle due to the alteration of refractive index of 0.01 is barely visible hence not measurable. Consequently, the refraction angle detection method can only achieve detection resolution of 0.02. The refraction angle detection method for refractive index sensing is not recommended for further improvement unless a novel method is introduced to incorporate position sensitive detector (PSD) into the

PDMS based planar optofluidic device. The PSD will provide higher sensitivity in detecting the change of refraction angle. PSD should be placed near the central axis where the refraction angle is detected. The challenge is how to integrate PSD seamlessly into the planar PDMS devices.

4.4 Recommendation and conclusion

The refractive index sensor demonstrated based on partial refraction provides a few distinct advantages that the traditional sensing techniques lack. The optofluidic refractive index sensor based on partial refraction offers direct integration within the planar microfluidic circuit and label-free fast refractive index sensing capability. The fluid-solid interface represents the horizontal axis for angle measurement and no calibration is needed to obtain the experimental pictures except setting the exposure time of the shutter to 30ms. The refractive index sensor based on partial refraction can provide fast sensing because it uses label-free sensing technique where there is no need for sufficient light to induce biochemical reaction with the fluid analyte solution in the detection process. The combination of the aforementioned two advantages cannot be offered by the traditional refractive index sensing devices [7-8][11-12][27]. The presence of fluorescent dye in the upper cladding microchannel and PDMS illuminates the lightpath for the light transmitting within the microchannel and the surrounding PDMS. The addition of fluorescent dye in the calcium chloride solution and the PDMS does not change the refractive indexes of both mediums. If the optofluidic refractive index sensor based on partial refraction is used for detecting the refractive index of the biological sample, the addition of fluorescent dye into the upper cladding microchannel may not be applicable as the biological sample may be sensitive to the presence of

fluorescent dye. Consequently, the refractive index sensing based on partial refraction cannot be applied. However, the sensing of the refractive index fluid analyte containing the biological sample can be achieved by measurement of the refraction angle from the lightpath within the dyed PDMS. The detection scheme based on measurement of refraction angle ensures the biological sample within the fluid analyte remains at its original state when it is undergoing refractive index sensing. The two refractive sensing schemes make use of the solid-liquid interface which does not need the constant supply of fluid analyte. This reduces the consumption of the fluid analyte substantially. The cavity within the upper cladding microchannel only needs 25 μl of fluid analyte to be filled completely. The elimination of fluid-fluid optical interface avoids high Reynolds number mixing. Meanwhile, it also eliminates the requirement for the refractive index sensor [73] to form liquid-core liquid-cladding optical interfaces during the optical detection. The detection scheme based on partial refraction also shortens the time needed for the refractive index detection because the injection of fluid analyte consume much shorter time than the time needed for the stabilization of the liquid-core liquid-cladding optical interface. The width of the microchannel used for sensing purpose is 120 μm which is the same dimensional scale as many other microfluidic circuits with different functionalities. The miniaturization of the optofluidic refractive index sensor based on partial refraction will facilitate its integration with many other microfluidic functionalities to realize μ-TAS systems based on single layer microfluidic circuits. The maturity of the fabrication technology also facilitates the rapid prototyping process of various lab-on-a-chip applications. The resolution of the fabrication based on quartz mask is 3 μm, hence the sidewalls of the microfluidic channels are optically smooth which lessen the optical scattering. The

refractive index sensing scheme based on refraction angle and its refractive index sensing capability can be above the value of 1.45. The criterion for the realization of the expansion of the sensing range for the refractive index is to have the incoming laser beam with incidence angle of 70˚. By measuring the refraction angle of the light after refraction at the solid-fluid optical interface, the refractive index of the fluid analyte can be calculated. For the refractive index sensing range between 1.37 and 1.45, the results obtained from the sensing scheme based on partial refraction and sensing scheme based on refraction angle can be put together for a comparison to improve consistency.

This chapter of the thesis has presented an optofluidic refractive index sensor based on partial refraction. The characterization of the optical reflection constant based on partial refraction and the measurement of refraction angle of the fluid analyte at different refractive index becomes the key indicators to identify the refractive index of the fluid analyte. The refractive index sensing resolution is 2×10^{-2} and 1×10^{-2} for the detection scheme based on optical reflection constant and refraction angle, respectively. The sensing resolutions are lower than the previous literatures [8][9][11][27] but they achieved the refractive index sensing resolution via surface plasmon resonance [7]. The optofluidic refractive index sensor in this chapter of the thesis is a promising tool to be integrated together with other functionalities to realize actual lab-on-a-chip sensing applications based on the optical principle of partial refraction. In the chapter 2 and 3, the optical principle of optical refraction and the incorporation of micromixer have led to the development of optofluidic compartments with much longer life time. The commonality among the studies made in the chapter 2, 3 and 4 is based on optical refraction on flat optical surfaces. Using the same optical principle of optical refraction, different optical manipulation

capabilities are achieved by incorporating curvature to the optical surfaces which lead us to the studies of optical diverging, collimating and focusing in chapter 5.

Chapter 5

Optofluidic variable-focus lenses for light manipulation

5.1 Concept and optical principle for the optofluidic variable-focus lenses

Utilizing the optical principle or optical refraction used in the past three chapters, an optofluidic device is created by applying curvature to the optical surfaces. The optofluidic devices that rely on the liquid-core liquid-cladding optical interface [4][34][22][32][66][74-77]can be reconfigured based on the shape of the optical interfaces and the refractive indexes of the liquids flowing within the microchannels. Although the tunability on these two parameters helps to create highly flexible optical devices, these benefits exist at the expenses of some limitations. These limitations include the short life time of the optofluidic devices. Furthermore, the optofluidic devices based on pure fluids interfaces can function provided that the fluids are constantly consumed. The life time of the optofluidic device is defined as the period of time it can function before the fluids needed to form the optical interfaces are totally consumed. The requirement of the optofluidic devices to be constantly supplied with liquid has shortened its life time considerably. The optofluidic devices [4][34][32-33][66][74] which the optical manipulation capabilities rely on laminar liquid-liquid optical interfaces or liquid-liquid optical interfaces with gradient refractive index (GRIN) [75] are affected by multiple factors, including micro particles, alteration of liquid flow rates and liquid pressure, and micro bubbles.

The occurrence of these factors will affect the stability of the liquid-liquid optical interfaces whether it is under laminar flow condition or diffusion between the liquid-liquid interfaces. When the stability of the liquid-liquid interfaces is affected, the optical manipulation capabilities may be disrupted. Solid/rigid optical devices [78-80] will not be affected by the aforementioned factors. It is because solid/rigid optical systems do not use the liquid-liquid laminar optical interfaces or liquid-liquid diffusion optical interfaces to achieve optical manipulation. However, solid/rigid optical devices cannot be optically tunable. Solid/rigid optical devices have much longer life time than optofluidic devices that make use of fluid-fluid optical interfaces. The optofluidic variable-focus lenses discussed in this chapter bring the strength in the pure fluid and pure solid based optics devices together including the optical tunability of the optofluidic lenses. At the same time, this innovation also reduces the limitations of both major classes of optical devices which include the short life time and low optical stability. The optical tuning accompanying the micromixing process is achieved by altering the refractive index of the fluid within the cavity of micrometers scale. After the optical tuning via alteration of refractive index of the fluid is completed, no further micromixing process is required. This feature has saved a lot of fluid as the fluid consumption can be reduced considerably. If there are microparticles and microbubbles residing within the optofluidic circuit, they can be extracted out of the microfluidic circuit by replacing the fluid within the microchannels. Meanwhile, the optical manipulation capability is not adversely affected. The absence of the fluid-fluid optical interfaces and the disruption of laminar flow due to high Reynold number micromixing lead to a highly stable optofluidic device that functions stably under unfavorable

circumstances. In this chapter, optofluidic variable-focus lenses for light manipulations [81] are investigated for its tunable light diverging, collimating and focusing capabilities. The optofluidic variable-focus lenses are realized in MOFS which provide all three lens' light manipulation functionalities within one optical device. The combination of all on-chip light manipulation capabilities in a single miniaturized microchip helps the integration of optofluidic lenses into a broad series of applications related to lab-on-a-chip or bio-photonic chip. During the process of fabricating the PDMS chips, once the chips are bonded after plasma treatment, no additional microfluidic or optofluidic circuits can be added into the chips. Consequently, it is an advantage to miniaturize all three on-chip light manipulation capabilities into a single microchip to extend the flexibility of the optofluidic variable-focus lenses. The solid/rigid optical device cannot achieve optical tunability and only has a single light manipulation capability.

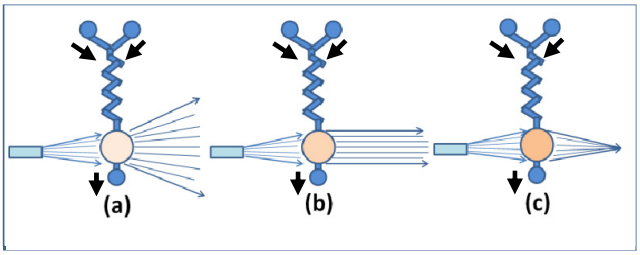

Figure 5.1 Tunable lens with surface radius of 214μm, lens thickness of 428μm (a) The optofluidic variable-focus diverging lenses with refractive index of 1.33. (b) The optofluidic variable-focus collimation lenses with refractive index of 1.54. (c) The optofluidic variable-focus focusing lenses with refractive index of 1.63.

The optofluidic variable-focus lenses for light manipulation has a long life time. In addition, the much improved optical stability due to the elimination of liquid-liquid optical surfaces and the integration of all three different light manipulation functionalities in a single microfluidic chip acquire distinct

advantages for bio-sensing and excitation applications. Figure 5.1(a-c) depicts the schematics for each optofluidic variable-focus lenses with different optical manipulation capabilities. The optofluidic lenses are attached together with a micromixer to enable the refractive index tuning. The micromixer is fed with two different kinds of fluids from two microchannel inlets. These two different kinds of fluid are isopropanol with refractive index of 1.33 and benzothiazole with refractive index of 1.63. These two different fluids are misible, enable the mixing of two fluids in all proportions. This allows the tuning of refractive index between 1.33 and 1.63 by altering the relative flow rates between the two microfluidic inlets. Within the tuning range of 0.3, three different optical manipulation capabilities can be realized including tunable optical diverging, collimating and focusing. Consequently, the optofluidic variable-focus lenses can strengthen or lessen the optical power at the detection optical fiber. The radius of curvature for the optofluidic variable-focus lens is 214 μm. Under the condition that the thickness of the lens is comparable to the optofluidic lens focal length, the focal length can be calculated from the Equation 5.1 [82] depicted below:

$$\frac{1}{f}=\left(\frac{n_l}{n_p}-1\right)\left(\frac{1}{R_l}-\frac{1}{R_r}+\left(\frac{\frac{n_l}{n_p}-1}{\frac{n_l}{n_p}}\right)\frac{t}{R_l R_r}\right) \qquad \text{(Equation 5.1)}$$

n_l and n_p reprsent the refractive indexes of the fluids residing within the lens cavity and the refractive index of the PDMS, respectively. R_l and R_r represent the radius of curvature of the optofluidic variable-focus lens on the left and right solid-fluid optical interface of the lens cavity. When the refractive index of the fluid within the lens' cavity is higher than the refractive index of the PDMS solid, the

optofluidic variable-focus lens is able to collimate the incoming laser beam. On the other hand, if the refractive index within the lens cavity is less than the refractive index of the solid PDMS, tunable optical diverging functionality is realized. The optofluidic variable-focus lens functions as the laser beam diverging lens. When the refractive index of the fluid within the lens cavity is tuned at 1.54, the optofluidic variable-focus lens functions as the laser beam collimator. As the refractive index of the fluid within the lens' cavity is tuned at 1.63, the optofluidic variable-focus lens functions as the focusing lens as shown in Figure 5.1(c). The realization of three different optical manipulation capabilities is due to the combination of the radius of curvature at the solid-fluid interface within the lens' cavity and the distance of the incoming optical fiber from the centre of the lens. The distance of the optical fiber connecting to the light source is crucial. If it is placed out of the focal length of the optofluidic variable-focus lens, then it can only provide optical collimating and focusing functionalities. The tunable optical diverging capability can only be realized when the optical fiber connecting to the Argon Ion laser light source is placed within the focal length of the optofluidic lens. The optical collimating and focusing capabilities are retained within the same optofluidic circuit. From the equation of the thick lens formula, the calculations show the focal length of the lens are -1270 μm, 1740 μm, and 877 μm when the refractive index of the fluid within the lens cavity is tuned at 1.33, 1.54 and 1.63, respectively. The wide tuning range of refractive index of 0.3 helps to scale down the optofluidic variable-focus lenses into optical device measured in micrometers. As the laser beam penetrate through the lens cavity filled with fluid with tunable refractive index, the Snell's Law in optics can be applied for analysis when the laser beam is refracted at the solid-fluid optical interfaces of the lens cavity.

5.2 Microchip fabrication and optical experimental setup

The device structures of the optical device are made using single exposure soft lithography process on a piece of silicon wafer. The height of the microstructures is 80 μm. The height of the microstructures decides the depth of the microchannels as the fabricated microstructures on the silicon wafer serve as the negative mold for PDMS moulding and casting. The fabrication based on quartz mask has the smallest resolution of 3 μm while the smallest microstructure within the design layout is 50 μm. The minimum size of the microstructure is approximately 16.6 times the resolution of the quartz mask. Consequently, the microstructures fabricated by the soft lithography process produce smooth microstructures sidewalls. This translates into optically smooth microchannels after PDMS casting and peeling for the reduction of optical losses at the fluid-solid interface.

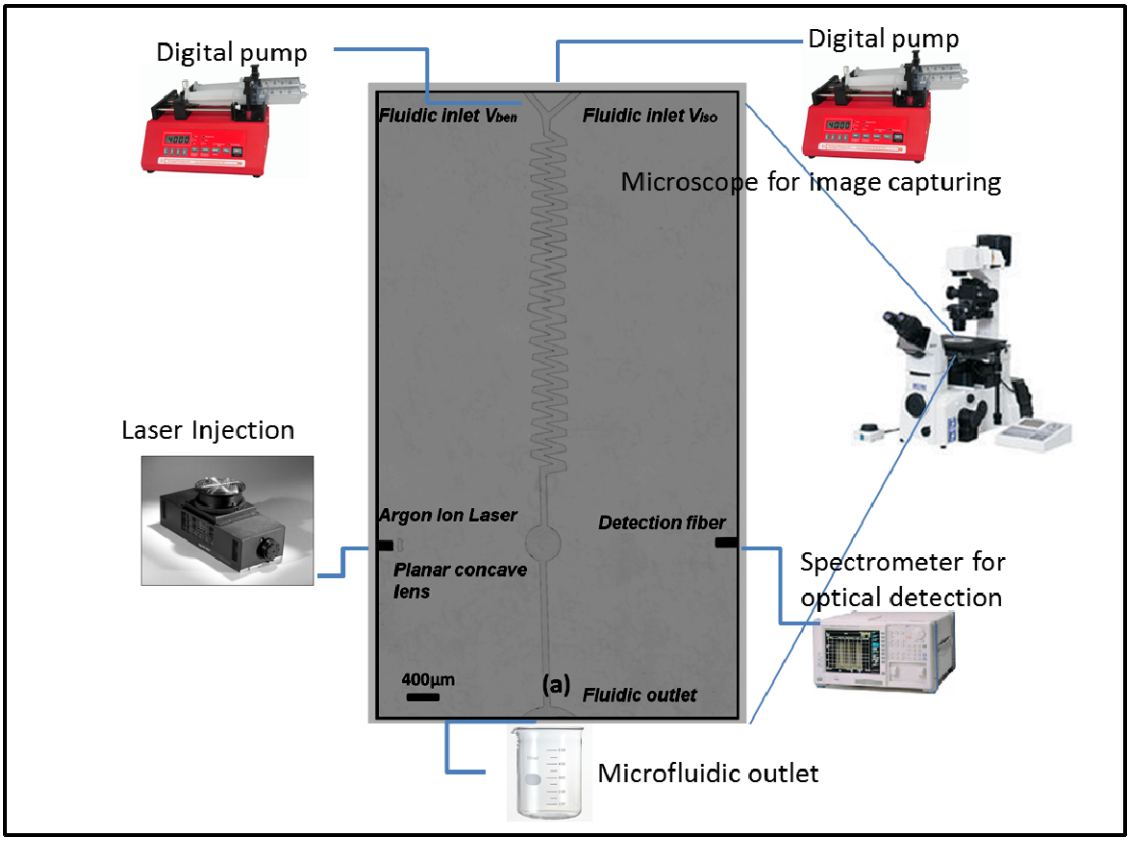

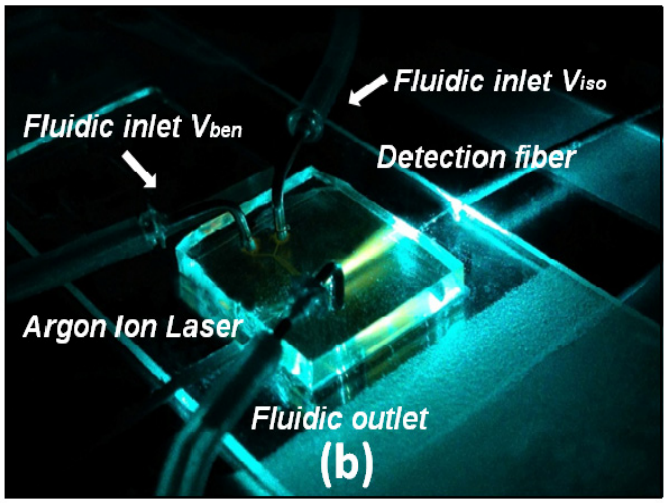

Figure 5.2 (a) Optofluidic circuit for the variable-focus lenses (b) Microfluidic chip under optical experiment

As the height of the microchannel is fixed at 80 μm and the smallest size of the microchannel is 50 μm, the smallest width to height ratio within the design is 0.625. To produce the dyed PDMS, Rodhamine 6G (Sigma-Aldrich) in powder form is mixed with methanol at 300:1 weight ratio. Rodhamine 6G has excitation and emission wavelength peaks at 526 and 555 nm. The uncured elastomer and its curing agent of PDMS are mixed at 10 parts to 1 part weight ratio. Finally, the uncured PDMS is mixed with the solution of Rodhamine 6G dissolved in methanol at 100 parts to 1 part weight ratio. The Rodhamine 6G solution is mixed with the PDMS subsequently. In the process of stirring, enormous amount of bubbles in different size would be produced in the uncured dyed PDMS. The uncured dyed PDMS is then subjected to degassing within the vacuum chamber to remove all the bubbles as the bubbles will increase its size when the bubbles move up in vertical direction in the uncured PDMS. The bubbles within the cured PDMS may block the view of the optofluidic circuit within the microchip. In other cases, the bubbles may destroy the PDMS microchannel when it is close enough to get in contact with the optofluidic circuit. After the degassing is completed, the uncured PDMS is

subjected to room temperature at 25°C for the period of 48 hours to complete the curing process. The curing process at higher temperature would lead to different refractive index than 1.45. The 48 hours of curing time at room temperature would yield the refractive index of 1.45 for Argon ion laser at 488nm wavelength of light.

The hardened PDMS is separated from the silicon wafer and extracted out of the mold. Three 0.5mm round shaped holes are drilled for the PDMS chip to allow the fluid to be injected into the microchannels via two microfluidic inlets and a single microfluidic outlet. The processed PDMS slab with holes then undergoes plasma treatment (March plasma system PX-250, March Instruments Inc.) in rendering the surface hydrophobic to be bonded with glass slide. The plasma treated PDMS chip and the glass slide are put into the plasma treatment machine with the bonding side facing upwards. Once the plasma treatment is completed, the two bonding sides are pressed against one another to squeeze out any air in between. The bonded chip is then placed in the oven at 65°C for 48 hours to complete the bonding process. The bonded chip which the PDMS sticks tightly with the substrate glass slide is then ready for the optical experiment. The optofluidic circuit is formed by the combination of micromixer with lens cavity. Figure 5.2(a) shows that the micromixer is constructed by many microchannels with zigzag shape having the channel width of 70 μm. Benzothiazole solution is chosen as the liquid with the maximum refractive index of 1.63 which is highest as compared to all other fluids. At the highest refractive index, benzothiazole remains optically transparent which the light can penetrate through without optical absorption. Benzothiazole does not cause any swelling within the PDMS microchip. The benzothiazole and isopropanol are able to mix in any proportions and they are injected into the PDMS microchip via two microfluidic inlets. The flow speed from the microfluidic inlets carrying

benzothiazole and isopropanol are depicted as V_{ben} and V_{iso}, respectively in Figure 5.2(b). Figure 5.2(a) shows that the tuning of refractive index of the solution is achieved by the micromixing process based on diffusion occurring at the 42 bends at the zigzag shaped microchannels. The benzothiazole solution with uniform refractive index flows into the lens' cavity from the micromixer and flows out of the microchip via the microfluidic outlet. The delivery of the fluid for the microchip is realized by connecting the tube (5212-B-90, EFD) and the silicone tubing (06411-59, Cole Parmer). The metal tube is connected to the microchip via the three 0.5mm holes drilled beforehand. The diameter of the metal tube is slightly larger than the 0.5mm hole, forming a secured sealing between the tube and the microchip due to the elastic property of the PDMS material. The luer to carb connector (X-012X, CONNEX) which can be connected and provided with fluid injection by the syringe is connected with silicone tubing. The syringe is placed in a digital pump to drive the fluid via different pressures exerted on the syringe to achieve different fluid flow speeds. The integration of silicone tubing, tube, connector, digital pump, and syringe has realized a liquid delivery system. Due to the tight sealing for each component, the liquid delivery system can function without fluid leakage. The smallest gap in the microchannels is 46 μm, ensuring that the bonding strength between the microchip and the glass substrate is strong. The width to height ratio for the 46 μm gap is 0.575. It ensures sufficient bonding strength between the two surfaces which prevent the fluid flowing within the microchnanels from fluid leakage. If the width to height ratio of the microchannel is too small, the bonding strength will be weak and may cause fluid leakage when the microchannels are subjected to high fluid pressure. The height of the microstructures on the silicon wafer is the same as the depth of the microchannels

in the PDMS microchip. There is a fiber insertion slot within the optotluific circuit to couple the laser beam into the optofluidic chip. The optical fiber (Silicon Lightwave Technology) with outer and core diameter of 125 μm and 62.5 μm, has the numerical aperture of 0.22. It is then inserted into the PDMS chip via the fiber insertion slot for the optical experiments. The optofluidic variable-focus lens can functions as tunable diverging, collimating and focusing lens. The optofluidic circuit includes a planar convex lens which the cavity within the lens is air. Figure 5.2(a) shows that the planar convex lens is situated 95 μm away from the tip of the optical fiber with radius of curvature of 110 μm to reduce the laser beam's diverging angle. The angle between the optical fiber and the optofluidic lens' cavity is 90°. Before the insertion of the optical fiber into the fiber insertion slot, the optical fiber is cut by the high precision cleaver (CT-30A, Fujikura) to render the tip of the optical fiber flat so that there is no cavity between the fiber insertion slot and the optical fiber. This would help to reduce the optical scattering which leads to optical losses. The same procedure is applied to the detection optical fiber placed at the opposite end of the optofluidic lens for detection of optical power. The detection optical fiber is connected to a high resolution spectrometer (HR4000, Ocean Optics Inc.). The optical fiber carrying 488nm Argon ion laser beam (532-AP-A01, Melles Griot) with beam power rated at 150mW is coupled into the microchip. The position of the optical fiber connecting to the light source is measured at 1600 μm away from the centre of the lens' cavity. At refractive index of 1.63, the focal length is calculated to be 877μm according to the thick lens formula. The laser should focus at 1940μm, hence the detection fiber is placed at 1950μm away from the centre of the lens. The micromixer functions as the tuner of refractive indexes by mixing the benzothiazole and isopropanol solution at different fluid flow rates.

The tuning of refractive index has led to the tuning of optical power. The optical power is detected by a high resolution spectrometer (HR4000, Ocean Optics Inc.). The two different kinds of liquid of benzothiazole and isopropanol with refractive index of 1.63 and 1.33 are pumped into the optofluidic circuit, entering the micromixer to yield a diluted benzothiazole solution with uniform refractive index. The experimental pictures from the experiment are recorded using the charge-coupled digital camera (DP70, Olympus) connecting with the inverted microscope (TE2000-E, Nikon). The measurements of the optical power for the optofluidic variable-focus lenses are repeated twenty times for each configuration of the lens' refractive indexes for the calculation of the average optical power. The focal plane of the microscope is adjusted to the middle height of the optofluidic circuit to obtain sharp microscope images.

5.3 Optofluidic variable-focus lenses experimental results and analysis

The reference optical power and beam width are measured when the refractive index of the diluted benzothiazole is tuned at 1.45. The optical powers detected with the optofluidic variable-focus lens at different refractive indexes divided by the aforementioned reference optical power would be the 'normalized power'. The normalized power guages the light intensity detected when the optofluidic variable-focus lens is tuned to achieve different optical manipulations. The loss of light caused by the light being scattered at two solid-fluid interfaces, optical absorption by the fluid within the cavity and the divergence of the laser beam is 5%. The optical losses due to the light scattered at the solid-fluid interfaces and the optical absorption due to the presence of benzothiazole solution in the lens' cavity do not acount for a large portion of the overall optical losses. The primarily cause of the

optical losses in the optofluidic circuit is the laser beam diverged when the optical pathlength increases. The proportion of light losses occur due to the fluid-solid interfaces is minimal as the sidewalls of the optofluidic circuit is optically smooth based on lithography technology with maximum resolution of 3μm. The experimental picture of the optofluidic variable-focus lens when the lens' cavity is filled with isopropanol at refractive index of 1.33 is shown in Figure 5.3(a). The lower refractive index of the isopropanol solution at 1.33 compared to the PDMS refractive index of 1.45 rendered the optofluidic lens a laser beam diverging lens. The percentage of increment of the beam width is the beam width when the refractive index of the optofluidic variable-focus lens ranges between 1.33 to 1.63, compared to the beam width when the refractive index of the optofluidic lens is at 1.45. The beam width is the vertical height of the laser beam at the detection fiber represented by the dotted lines in Figure 5.3(a-b). The beam width is measured by magnifying the experimental picture by five times and measuring it according to the scale bar. Each measurement is conducted 20 times to obtain the average beam width. The highest standard deviation for the beam width is 18.75μm for sample size of 20. The optical attenuation of the laser beam diverging lens causes the laser beam width to be widen by 113%.

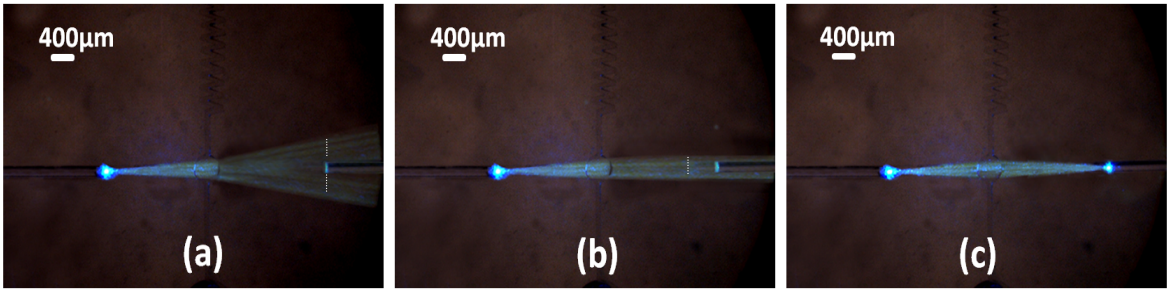

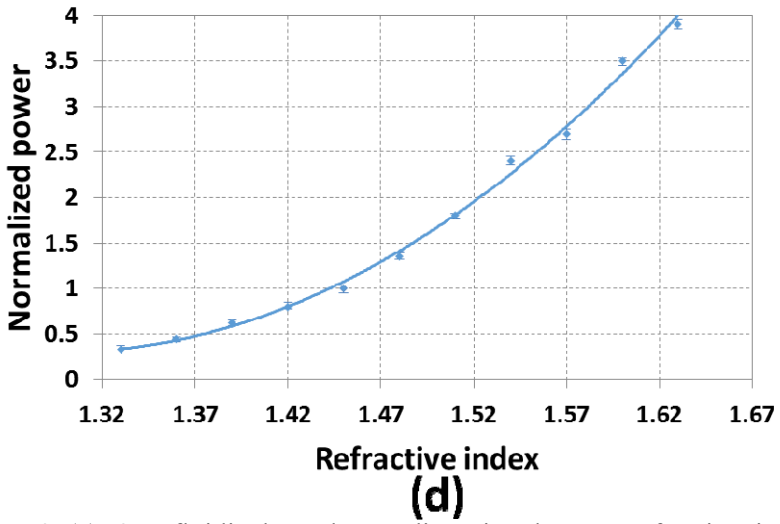

Figure 5.3 (a) Optofluidic laser beam diverging lens at refractive indexes of 1.33 (b) Optofluidic collimator at refractive index of 1.54 (c) Optofluidic focusing lens at refractive indexes of 1.63 (d) The correlation between the refractive indexes of the fluid within the lens' cavity and the normalized power.

The optofluidic laser beam diverging lens as shown in Figure 5.3(a) has normalized power of 0.33, comparing to the optical power of the detection fiber when the optofluidic variable-focus lens is tuned at refractive index of 1.45. The lower refractive of the isopropanol solution within the lens' cavity increase the divergence of the laser beam which leads to the lowering of the optical power. The optical losses due to the adsorption of diluted benzothiazole solution for the Argon Ion laser light source (488nm) is minimal as the optical absorption range of the benzothiazole ranges from optical wavelength of 220nm and 290 nm. Besides functioning as a laser beam diverging lens, the optofluidic variable-focus lens can also increase the detected optical power. When the lens' cavity is injected with benzothiazole solution with refractive index of 1.54, the laser beam undergoes optical collimation with normalized power of 0.62. The reduction of beam width is coupled with the normalized power of 2.4 compared to the laser beam with normalized power of 1 when the lens' cavity is tuned at refractive index of 1.45. In order to allow the optofluidic variable-focus lens functions as a focusing lens,

benzothiazole solution at refractive index of 1.63 is injected into the lens' cavity. As the refractive index of the benzothiazole solution is higher than the PDMS refractive index at 1.45, the solid-fluid interfaces focus the laser beam leading to normalized power of 3.9 comparing to the laser beam without any manipulation when the lens' cavity is filled with benzothiazole solution at refractive index of 1.45. The capabilities of the optofluidic variable-focus lenses to function as a laser beam diverging lens, collimating and focusing lens are demonstrated. When the lens cavity is filled by fluid with refractive index from 1.33 to 1.45, the optofluidic variable-focus lens can function as a tunable laser beam diverging lens. The divergence angle can be adjusted when the refractive index of the lens' cavity is tuned from 1.33 to 1.45. The divergence angle of the laser beam is inversely proportional to the refractive index of the fluid within the lens' cavity. When the refractive index of the fluid filling the lens' cavity ranges from 1.45 to 1.63, the optofluidic variable-focus lenses function as optical collimating and optical focusing lens. The optically attenuated beam width is inversely proportional to the refractive index of the fluid residing within the lens' cavity.

Figure 5.3(d) shows the relationship between the normalized powers with respect to different refractive indexes of the optofluidic variable-focus lenses. When the fluid within the lens' cavity is tuned at the refractive index ranges from 1.33 to 1.45, the optofluidic variable-focus lens functions as a laser beam diverging lens. Consequently, the value of the normalized power is below 1. When the fluid within the lens' cavity is tuned at the refractive index ranges from 1.45 to 1.63, the optofluidic variable-focus lenses function as laser beam collimator and optical focusing lens. Consequently, the optofluidic circuit achieves normalized power that is beyond 1. When refractive index of the fluid within the lens' cavity is tuned at

1.33, the optical beam width is the largest, which leads to the lowest normalized power. However, when the refractive index of the fluid within the lens' cavity is tuned at 1.63, then normalized power is recorded to be 3.9. The highest standard deviation for the normalized power at different refractive indexes is 0.04025 for the sample size of 20. The signal to noise ratio for the measurement of optical intensity is 300:1. The normalized power is proportional to the refractive index of the fluid residing within the lens' cavity having a radius of curvature of 214 μm. The reduction of focal length can increase the divergence angle further and focus the laser beam at location nearer to the center of the lens. This would help to increase the dynamic tuning range of the optofluidic variable-focus lens, and the optofluidic circuit can achieve even higher magnification factor and divergence angle when the optofluidic circuit functions as laser beam diverging lens and optical focusing lens, respectively.

5.4 Refractive index tuning based on micromixing

The microfluidic inlet channels for fluid injection of benzothiazole and isopropanol for these two miscible fluids to undergo micromixing based on diffusion to produce diluted benzothiazole solution with different flow speeds at the two microfluidic inlets. The tuning range of refractive index ranges from 1.33 to 1.63 as shown in Figure 5.4 shows a linear relationship between the flow speeds and the resultant refractive indexes of the diluted benzothiazole solution. The total flow speed of within the optofluidic circuit is fixed at 90μl/min. The tuning of refractive index of the benzothiazole solution from 1.36 to 1.60 is repeated 20 times for each refractive index at an interval of 0.03. The standard deviation for the refractive index measurement based on micromixing at different flow speeds is 0.005304 for sample

size of 20. The measurement error for the refractive index sensing based on the highest resolution of the refractometer (Reichert, AR200) is 0.001. The measurement error the flow rate controlled by the digital pump is 0.1 μl/min. The micromixing process would consume 3.5 seconds for sufficient diffusion at 42 bends within the micromixer to achieve refractive index tuning from 1.36 to 1.60. The design of 42 bends within the micromixer is to allow sufficient path length for diffusion to occur and facilitate the micromixing process in yielding a homogenous diluted benzothiazole solution. The theoretical calculation shows that the Reynold number within the micromixer is approximately 6.06. As long as the Reynold number is not over 80 [50], the micromixing process is primarily driven by diffusion between two miscible fluids. The speed of micromixing can be hastened by utilizing higher total flow rates from the two microfluidic inlets. The amount of time consumed for the optofluidic circuit to reduce the refractive of the fluid residing within the lens' cavity from 1.63 to 1.36 takes 10 seconds. The optofluidic circuit consumes much longer period than 10 seconds for the reduction of refractive index of the lens from 1.63 to 1.36 due to the backpressure formed when the low viscosity benzothiazole solution is pushing the high viscosity benzothiazole solution out of the optofluidic circuit. The optofluidic circuit would consume 0.5 second to fill the lens cavity with isopropanol solution at refractive index of 1.33. Meanwhile, the time taken for the lens' cavity to be filled with benzothiazole solution, which is more viscous at refractive index of 1.63, is 0.8 seconds. The optofluidic circuit would consume 1.2 second to tune the refractive index of the fluid within the lens' cavity from 1.33 to 1.63 by replacing the low viscosity isopropanol solution with high viscosity benzothiazole solution. The optofluidic circuit would consume 4.5 seconds to tune the refractive index of the optofluidic

variable-focus lens from 1.63 to 1.33 by replacing the high viscosity benzothiazole solution with low viscosity isopropanol solution. The scattering of the laser beam happened in the process of optical tuning can be avoided by switching off the Argon ion laser light source. The optical tuning can be hastened by utilizing faster total flow speeds from the two microfluidic inlets.

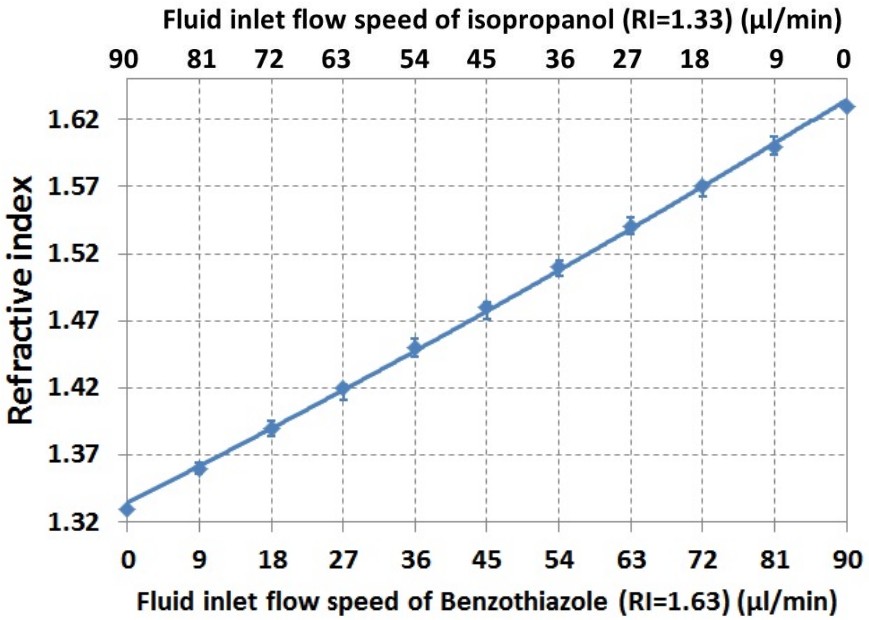

Figure 5.4 The resultant refractive index of the solution by mixing benzothiazole and isopropanol solution at varied flow rates

5.5 Enhanced fluorescence sensing via optofluidic variable-focus lens

The optofluidic circuit can be used to tune or enhance the fluorescence signal in its sensing application. The first preparation step for the fluorescence sensing is the mixing between the Rodhamine 6G (Sigma-Aldrich) and methanol at 1 part to 300 parts weight ratio. The subsequent step is the mixing between the aforementioned Rodhamine solution and isopropanol at 150 parts to 1 part weight ratio. Similarly, the Rodhamine solution is mixed with pure benzothiazole solution at the same weight ratio. The Rodhamine dyed isopropanol and benzothiazole solution are

injected into the micromixer to produce diluted dyed benzothiazole solution to be filled into the lens' cavity. In the preparation of the PDMS microchip, no fluorescent dye is used within the PDMS for reducing the disturbance of the fluorescence signal emitted by the PDMS at the detection optical fiber. The diluted dyed benzothiazole solution residing within the lens' cavity will emit light with wavelength of 555nm when the dyed solution is excited by laser beam with 488nm wavelength. The dye concentration within the isopropanol and benzothiazole solution is the same. The optofluidic circuit is able to tune with the optical output power of the fluorescence signal at the optical detection fiber by varying the refractive index of the dyed diluted benzothiazole solution. When the refractive index of the dyed diluted benzothiazole solution within the optofluidic lens is tuned from 1.45 to 1.63, the fluorescence signal is enhanced as the laser is collimated or focused before detected by the optical fiber. Figure 5.5 shows the relationship between the normalized power of the emission light at the optical detection fiber for refractive index of the benzothiazole solution at 1.63 and 1.45 for wavelength ranges from 500nm to 662nm. The aforementioned normalized power is divided by the optical power of the same wavelength when the refractive index of the benzothiazole solution is tuned at 1.45. When the dyed diluted benzothiazole solution is tuned at refractive index of 1.45, the optofluidic circuit does not attenuate the incoming laser beam. Figure 5.5 shows the blue color optical fluorescence signal spectrum recorded when the benzothiazole solution is at refractive index of 1.63, which achieves the normalized fluorescence optical power of 2.86. The optofluidic circuit demonstrated the capability to be a fluorescence sensor within the microchip that can be integrated with other microfluidic functionalities.

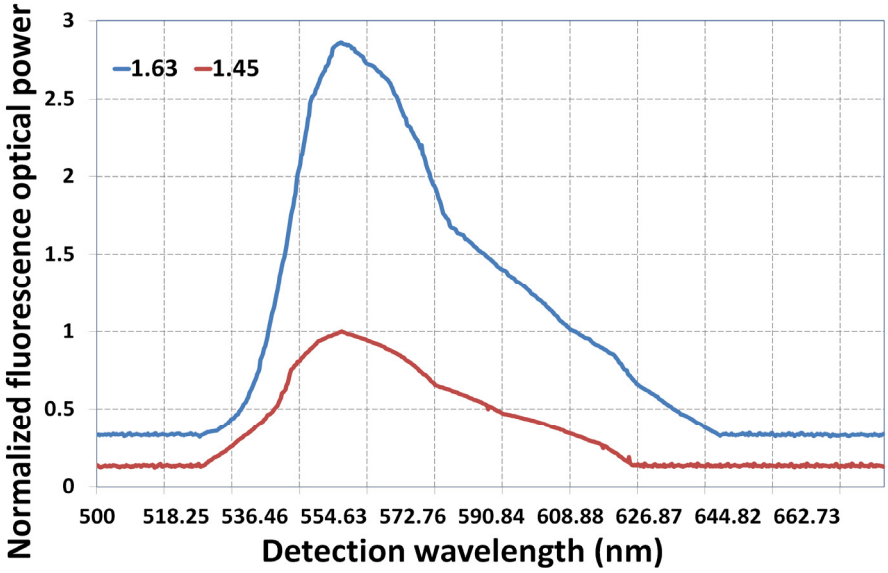

Figure 5.5 The emission spectrum of the dyed benzothiazole solution at refractive index of 1.63 (blue) and 1.45(red) with respect to wavelength ranges from 500nm to 662.73nm

The material used for construction of the microchip is PDMS elastomer. It has important optical characteristics of high transparency within the wavelength range of visible light. Consequently, the transmission of light within the PDMS does not suffer from optical losses due to adsorption of the transmitting medium. The optically smooth microchannels' sidewalls contributed by high resolution fabrication technology when combined with the PDMS as the material for constructing the microchip, lead to the low optical loss for light travelling within the optofluidic circuit. The optofluidic circuit demonstrated the ability to manipulate the optical power of the laser beam in planar PDMS microchip. It can be integrated with either high power or low power laser to reduce or enhance the optical power. Majority of the optical excitation and sensing applications do not need a fast optical tuning, hence the optofluidic circuit demonstrated is suited for integration with a broad range of bio-sensing applications including fluorescence microscopy, flow cytometry, and bioassays. The lens' cavity only requires 0.0115 µl of fluid to be filled completely. The optofluidic variable-focus lens is a static device rather than a dynamic device [66]. The maximum refractive index difference

between the lens' cavity filled with pure benzothiazole solution and the surrounding PDMS is 0.18. This amount of modulation in refractive index is 20 to 200 times higher than the refractive index modulation for the optical devices based on the physics of thermal and electro-optic. This enables the possible miniaturization of the optofluidic variable-focus lens to scale of tens of micrometers.

5.6 Recommendation and conclusion

As a conclusion, the optical manipulation capabilities of the optofluidic variable-focus lens are demonstrated including tunable optical diverging, collimating and focusing. By integrating the micromixer together with the optofluidic lens' cavity, the optofluidic circuit with tunable refractive index combines the advantages found in pure solid optical device and pure fluidic optofluidic compartment. The optofluidic circuit essentially combines the advantage of optical tunability derived from the pure fluid based optical devices and the advantage of high optical stability derived from the pure solid based optical devices. The utilization of solid-fluid optical interfaces has prolonged the life time of the optofluidic circuit significantly. The large tuning range of refractive index also helps to realize all optical manipulation techniques that render the optofluidic circuit to be a tunable laser beam diverging, collimator and focusing lenses. The alteration of the refractive indexes within the lens' cavity is achieved by adjusting the relative flow speeds from the benzothiazole and isopropanol fluid inlets. The integration of the optofluidic circuit into its corresponding lab-on-a-chip applications is easy and fast. The microchannels can be fabricated together with other microfluidic channels with different functions within a single layer of lithography on the silicon wafer. This has hastened the speed of rapid prototyping of the lab-on-a-chip devices. The

optofluidic circuit demonstrated is a potential optical compartment to be a highly flexible light manipulation system for all kinds of laser to achieve on-chip optical excitation. To increase the precision and performance of the optical tuning, compound lenses can be integrated in the optofluidic circuit. An on chip fluorescence sensor built on the optofluidic variable focus lens is demonstrated with tunable fluorescence intensity. The ultimate purpose of the optofluidic circuit is for bio-excitation and sensing application to achieve bio-analysis and bio-screening.

Chapter 6

Conclusion and Recommendation

In the study of optical reflectivity in chapter 2, the optical interfaces between core and cladding fluids are laminar and optically smooth. However, due to the limitation of fluid-fluid optical interface, solid-fluid optical interfaces are employed for studying of the optical reflectivity from chapter 3 to chapter 5. The shape of the optical interface is flat for chapter 2 to chapter 4 while the shape of the optical interface is curved for chapter 5. All optical manipulations or sensing capabilities developed are based on the manipulation of optical reflectivity at the optical interfaces. The optical properties of the fluid medium can be altered easily by replacing the fluids. Fluids based optical systems have unique properties that the solid counterparts cannot achieve. Seamless integration with applications and optical re-configurability are two major advantages of optofluidic compartments.

6.1 Major contributions of the dissertation

In the previous four chapters, optical manipulation and sensing based on optical reflectivity are studied via the creation of four optofluidic devices; each caters for different optical functionalities. In the studies within chapter 2 to chapter 4, when the optical surface is flat with tunable refractive index, the optical switching and optical sensing are realized. The optical switching via fluids injections simplifies the adoption of optofluidic switching device in microfluidic circuits significantly without any mechanical moving parts. In chapter 3, the solid-fluid interfaces employed for optical switching has a long life time while eliminating the weakness

of low optical stability of the optofluidic switch based on fluid-fluid interfaces. In chapter 4, the adaptation of refractive index sensing in microfluidic circuit is greatly simplified with the refractive index sensing scheme based on optical partial refraction. In chapter 5, when the curved optical surfaces are employed, optical manipulation capabilities including optical diverging, collimating and focusing are achieved. The optofluidic lens based on solid-fluid interfaces has a long life time while eliminating its major drawback of low mechanical stability for its fluid-fluid optical interfaces. Each optical manipulation capabilities is tunable as varying the refractive indexes within the optofluidic circuit can change the reflectivity of the optical surfaces. All the optofluidic devices for light manipulations are built without any mechanical components. The seamless integration of optofluidic compartments [83-88] in lab-on-a-chip research field has realized applied optics for potential optical excitation, sensing and switching applications like on-chip fluorescence sensing and flow cytometry.

6.2 Suggestions for future work

The trend of miniaturization of optofluidic devices and its integration in microfluidic platform would provide more opportunities for the development of on-chip bio-sensing or detection. These techniques can be implemented in biomedical applications. It is a burgeoning field with important applications in areas such as biotechnology and analytical chemistry, for instance, clinical analysis, analysis of solutions and particles, droplet manipulation and nutrition analysis. Many technological elements and fundamental concepts are being researched currently. The optofluidic and microfluidic devices fabrication uses standard soft-lithography to create complex microfluidic circuits. This allows rapid prototyping of

microfluidic devices. Below are two concepts that can bring new novel functionalities to lab-on-a-chip research community. Firstly, by realizing new optical phenomena with microfluidic or nanofluidic circuits, new optical excitation, sensing and switching capabilities can be created as the future works in the regime of nanophotonics and nonlinear optics. Secondly, the optofluidic research hold promises for the future of biomedical diagnoses but few designs have been commercialized. Each optofluidic device created in the literature should cater to a specific biomedical application.

References

1. D. Psaltis, S. R. Quake, C. H. Yang, “Developing optofluidic technology through the fusion of microfluidics and optics”, *Nature* **442** (2006) 381-386.
2. J. C. McDonald, D. C. Duffy, J. R. Anderson, D. T. Chiu, H. Wu, O. J. Schueller, G. M. Whitesides, "Fabrication of microfluidic systems in poly (dimethylsiloxane)" *Electrophoresis* **21 (**2000) 27-40.
3. L. K. Chin, A. Q. Liu, C. S. Lim and Y. C. Soh, “An on-chip liquid tunable grating using multiphase droplet microfluidics,” *Appl. Phys. Lett.* **93** (2008) 164107.
4. S. K. Y. Tang, C. A. Stan and G. M. Whitesides, “Dynamically reconfigurable liquid-core liquid-cladding lens in a microfluidic channel,” *Lab Chip.* **8** (2008) 395-401.
5. A. Groisman, S. Zamek, K. Campbell, L. Pang, U. Levy and Y. Fainman, “Optofluidic 1X4 Switch,” *Opt. Express.* **16** (2008) 13499-13508.
6. W. Z. Song, A. E. Vasdekis, Z. Y. Li and D. Psaltis, “Optofluidic evanescent dye laser based on a distributed feedback circular grating,” *Appl. Phys. Lett.* **94** (2009) 161110.
7. J. Ctyroky, J. Homola, P. V. Lambeck, S. Musa, H. J. W. M. Hoekstra, R. D. Harris, J. S. Wilkinson, B. Usievich, N. M. Lyndin, “Theory and modeling of optical waveguide sensors utilizing surface Plasmon resonance,” *Sens. Actuators B: Chemical* **54** (1999) 66-73.
8. K. Mitsui, Y. Handa, K. Kajikawa, “Optical fiber affinity biosensor based on localized surface plasmon resonance,” *Appl. Phys. Lett.* **85** (2004) 4231:1-4231:3.

9. W. Z. Song, X. M. Zhang, A. Q. Liu, C. S. Lim, P. H. Yap, H. M. M. Hosseini, "Refractive index measurement of single living cells using on-chip Fabry-Perot cavity", *Appl. Phys. Lett.* **89** (2004) 203901:1-203901:3.
10. X. C. Li, J. Wu, A. Q. Liu, Z. G. Li, Y. C. Soew, H. J. Huang, K. Xu, and J.T. Lin, "A liquid waveguide based evanescent wave sensor integrated onto a microfluidic chip," *Appl. Phys. Lett.* **93** (2008) 193901:1-193901:3.
11. D. Brennan, P. Lambkin, P. Galvin, "Refractive index measurement in a shallow multichannel microfluidic system", *Meas. Sci. Technol*. **19** (2008) 085403:1-085403:7.
12. Z. Y. Wang, J. R. Heflin, R. H. Stolen, S. Ramachandran, "Highly sensitive optical response of optical fiber long period gratings to nanometer-thick ionic self-assembled multilayers," *Appl. Phys. Lett*. **86** (2005) 223104:1-223104:3.
13. L. K. Chin, A. Q. Liu, C. S. Lim and Y. C. Soh, "An on-chip liquid tunable grating using multiphase droplet microfluidics," *Appl. Phys. Lett.* **93** (2008) 164107.
14. K. Zhou, X. Chan, L. Zhang, I. Bennion, "High-sensitivity optical chemsensor based on etched D-fibre Bragg gratings", *Electron. Lett*. **40** (2004) 232-234.
15. V. Bhatia, A. M. Vengsarkar, "Optical fiber long-period grating sensors", *Opt. Lett*. **21** (1996) 692-694.
16. S. K. W. Sia, G. M. Whitesides, " Microfluidic devices fabricated in poly(dimethylsiloxane) for biological studies," *Electrophoresis,* **24** (2003) 3563-3576.
17. G. M.Whitesides, "The origin and the future of Microfluidic," *Nature* **442** (2007) 368-374.

18. J. M. K. Ng, I. Gitlin, A. D. Stroock, and G. M. Whitesides, "Components for integrated Poly(dimethylsiloxane) microfluidic system," *Electrophoresis* **23 (**2002) 3461- 3473.
19. T. Sakata, H. Togo, M. Makihara, F. Shimokawa, and K. Kaneko "Improvement of Switching Time in a Thermocapillarity Optical Switch", *J. Lightwave. Technol.* **19** (2001) 1023-1027.
20. B. J. Li, Y. Zhang, L. H. Teng, Y. Z. Zhao "Symmetrical 1x2 digital photonic splitting switch with low electrical power consumption in SiGe waveguides", *Opt. Express.* **13** (2005) 654-659.
21. K. Campbell, A. Groisman, U. Levy, L. Pang, M. Shayan, D. Psaltis, and Y. Fainman "A microfluidic 2X2 optical switch", *Appl. Phys. Lett*. **85** (2004) 6119-6121.
22. D. B. Wolfe, R. S. Conroy, P. Garsteki, B. T. Mayers, M. A. Fischbach, K. E. Paul, M. Prentiss, and G. M. Whitesides, "Dynamic control of liquid-core/liquid-cladding optical waveguides", *Proc. Natl. Acad. Sci.* **101** (2004) 12434-12438.
23. J. M. Lim, J. P. Urbanski, T. Thorsen, and S. M. Yang "Pneumatic control of a liquid-core/liquid-cladding waveguide as the basic for an optofluidic switch", *Appl. Phys. Lett*. **98** (2011) 044101.
24. H. R. Gwon and S. H. Lee "Spectral and Angular Responses of Surface Plasmon Resonance Based on the Kretschmann Prism Configuration", *Mater. Trans.* **51** (2010) 1150-1155.
25. R. Micheletto and Y. Kawakami "Index-of-refraction sensors: virtually unlimited sensing power at the critical angle", *Opt. Lett.* **31** (2006) 205-207.
26. Y. Sarov, K. Ivanova, T. Ivanov, B. E. volland, and I. W. Rangelow "Microfluidic analysis based on total internal light reflection", *Microelectron. Eng.* **83** (2005) 1294-1297.

27. D. Brennan, P. Lambkin and P. Galvin, “Refractive index measurements in a shallow multichannel microfluidic system”, *Meas. Sci. Technol.* **19** (2008) 085403.
28. M. Agarwal, R. A. Gunasekaran, P. Coane and K. Varahramyan, “Polymer-based variable focal length microlens system,” *J. Micromech. Microengin.* **14** (2004) 1665-1673.
29. S. H. Ahn and Y. K. Kim, “Proposal of human eye’s crystalline lens-like variable focusing lens,” *Sens. Actuat A:Physical.* **78** (1999) 48-53.
30. L. Pang, U. Levy, K. Campbell, A. Groisman and Y. Fainman, “Set of two orthogonal adaptive cylindrical lenses in a monolith elastomer device,” *Opt. Express.* **13** (2005) 9003-9013.
31. H. Ren and S. T. Wu, “Variable-focus liquid lens by changing aperture,” *Appl. Phys. Lett.* **86**. (2005) 211107-1-211107-3.
32. X. Mao, J. R. Waldeisen, B. K. Juluri and T. J. Huang, “Hydrodynamically tunable optofluidic cylindrical microlens,” *Lab. Chip*. **7** (2007) 1303-1308.
33. Y. C. Seow, A. Q. Liu, L. K. Chin, X. C. Li, H. J. Huang, T. H. Cheng and X. Q. Zhou, “Different curvature of tunable liquid microlens via the control of laminar flow rate”, *Appl. Phys. Lett.* **93**. (2008) 084101.
34. M. Rosenauer and M. J. Vellekoop, “3D fluidic lens shaping-A multiconvex hydrodynamically adjustable optofluidic microlens”, *Lab. Chip*. **9** (2009) 1040-1042 .
35. M. J. C. Cram L S, J. A. Steinkamp, T. M. Yoshida, T. N. Buican, B. L. Marrone, J. H. Jett, G. Salzman and L. Sklar, "New flow cytometric capabilities at the National Flow-Cytometry Resource Proc," *IEEE,* **80** (1992) 7.
36. H. A. T. R. Wilson, R. Desilva and A. P. Schaap, "Electrochemiluminescence determination of 2′,6′- difluorophenyl 10-Methylacridan-9-carboxylate," *Analytical Chemistry* **73** (2001) 763-767.

37. G. B. L. C.H. Lin, Y. H. Lin and G.L. Chang, "A fast prototyping process for fabrication of microfluidic systems on soda-lime glass," *Journal of Micromechanics and Microengineering* **11** (2001) 726-733.
38. P. C. Li, and D. J. Harrison, "Transport, manipulation, and reaction of biological cells onchip using electrokinetic effects," *Analytical Chemistry* **69** (1997) 1564-1568.
39. A. Y. Fu, C. Spence, A. Scherer, F. H. Arnold and S. R. Quake, "A microfabricated fluorescence-activated cell sorter," *Natural Biotechnology* **17** (1999) 1109-1111.
40. N. Nguyen and S. Wereley, "Fundamentals and Applications of Microfluidics," *Artech House,* 2000.
41. A. V. Lemoff and A. P. Lee,"An AC magnetohydrodynamic micropump," *Sensors Actuators B* **63** (2000) 178-185.
42. M. A. McClain, C. T. Culbertson, S. C. Jacobson and J. M. Ramsey, "Flow cytometry of Escherichia coli on microfluidic devices," *Analytical Chemistry* **1** (2001) 5334-5338.
43. X. L. Mao, S. C. S. Lin, C. Dong, and T. J. Huang "Single-layer planar on-chip flow cytometer using microfluidic drifting based three-dimensional (3D) hydrodynamic focusing", *Lab Chip* **9** (2009) 1583-1589.
44. K. W. MRCP. Muir, L. B. M. McNeish, G. M. D. Donald, M. M. D. Metcalfe, "Visualization of cardiac emboli from mitral valve papillary fibroelastoma", *Journal of Cerebral Circulation* **27(6)** (1996) 1133.
45. R. P. Wersto, E. R. Rosenthal, R. G. Crystal, and K. R. Spring, "Uptake of fluorescent dyes associated with the functional expression of the cystic fibrosis transmembrane conductance regulator in epithelial cells.", *Proc. Natl. Acad. Sci.* **93** (1996) 1167-1172.

46. J. P. Brody, P. Yager, R. E. Goldstein, and R. H. Austin, "Biotechnology at low Reynolds numbers," *Biophys. J.* **71** (1996) 3430.

47. R. H. Carlson, C. V. Gabel, S. S. Chan, R. H. Austin, J. P. Brody, and J. W. W. M. James, "Seld-sorting of white blood cells in a lattice," *Phys.Rev. Lett.* **79** (1997) 2149.

48. A. V. J. B. Knight, J. P. Brody and R. H. Austin, "Hydrodynamic focusing on a silicon chip: mixing nanoleters in microseconds," *Physical Review Letter* **80** (1998) 3863-3866.

49. O. H. Miyake R, Yamazaki I and Takagi T, "Investigation of sheath flow chambers for flow cytometers (micro machined flow chamber with low pressure loss)," *JSME Int. J.B.* **40 (**1997) 106-113.

50. O. H. Miyake R, Yamazaki I and Takagi T, "Flow cytometric analysis by using micro-machined flow chamber," *JSME Int. J. B* **43 (**2000) 219-224.

51. B. G. R. J. Hodder P S, "Microfabricated flow chamber for fluorescence-based chemistries and stopped-flow injection cytometry," *Analyst* **122** (1997) 883-887.

52. M. Koch, A. G. R. Evans, and A. Brunnschweiler, "Design and fabrication of a micromachined Coulter counter," *J. Micromech. Microeng.* **9** (1999) 159-161.

53. Y. A. Sobek D, Gary M L and Senturia S D "A microfabricated flow chamber for optical measurements in fluids Proc," *6th IEEE MEMS (*1993) 219-224.

54. H. L. Che and G. B. Lee, "Micromachined flow cytometers with embedded etched optics fibers for optical detection," *J. Microeng* **13** (2003) 447-453.

55. C. C. T. Schrum D P, Jacobson S C and Ramsey J M "Microchip flow cytometry using electrokinetic focusing," *Anal. Chem* **71** (1999) 4173-4177.

56. Z. M. Tung Y C, Lin C T, Kurabayashi K and Skerlos S J, "PDMS-based opto-fluidic micro flow cytometer with two-color, multi-angle fluorescence detection capability using PIN photodiodes," *Sensors Actuators* **98** (2004) 356-367.

57. T. Y. C. Huh D, Wei H H, grotberg J B, Skerlos S J, Kurabashi K and Takayama S "Use of air-liquid two-phase flow in hydrophobic microfluidic channels for disposable flow cytometers " *Biomed Microdevices* **4 (**2002) 141-149.

58. L. Cui, T. Zhang, and H. Morgan, "Optical particle detection integrated in a dielectrophoretic lab-on-a-chip " *J. Micromech. Microeng.* **12** (2000) 7-12.

59. S. K. Kruger J, O'Neill A, Jackson C, Morrison A and O'Brien P, "development of a microfluidic device for fluorescence activated cell sorting," *J. Micromech. Microeng.* **12** (2002) 486-94.

60. A. Y. Fu, C. Spence, A. Spherer, F. H. Arnold and S. R. Quake, "A microfabricated fluorescence-activated cell sorter," *Nat Biotechnol.* **17** (1999) 1109-1011.

61. D. A. B. Miller, D. S. Chemla, T. C. Damen, A. C. Gossard, W. Wiegmann, T. H. Wood and C. A. Burrus, "Novel hybrid optically bistable switch: The quantum well self electro-optic effect device," *Appl. Phys. Lett.* **45** (1984) 13-15.

62. S. K. Korotky, G. Eisenstein, R. S. Tucker, J. J. Veselka and G. Raybon, "Optical intensity modularot rto 40Ghz using a waveguide electro-optic switch", *Appl. Phys. Lett.* **50** (1987) 1631-1633.

63. Y. C. Seow, S. P. Lim, H. P. Lee, "Tunable optofluidic switch via hydrodynamic control of laminar flow rate", *Appl. Phys. Lett.* **95** (2009) 114105.

64. A. V. J. B. Knight, J. P. Brody and R. H. Austin, "Hydrodynamic focusing on a silicon chip: mixing nanoleters in microseconds", *Physical Review Letter* **80** (1998) 3863-3866.

65. H. A. T. R. Wilson, R. Desilva and A. P. Schaap "Electrochemiluminescence determination of 2′,6′- difluorophenyl 10-Methylacridan-9-carboxylate", *Analytical Chemistry* **73** (2001) 763-767.

66. Mao X L, Lin S C S, Lapsley M I, Shi J J, Juluri B K and Huang T J "Tunable liquid

gradient refractive index (L-GRIN) lens with two degrees of freedom", *Lab Chip* **9** (2009) 2050-2058.

67. S. K. Y. Tang, Z. Y. Li, A. R. Abate, J. J. Agresti, D. A. Weitz, D. Psaltis and G. M. Whitesides "A multi-color fast switching microfluidic droplet dye laser", *Lab chip* **9** (2010) 2767-2771.
68. H. Huang, X. L. Mao, S. C. S. Lin, B. Kiraly, Y. P. Huang and T. J. Huang "Tunable two-dimensional liquid gradient refractive index (L-GRIN) lens for variable light focusing", *Lab Chip* **10** (2010) 2387-2393.
69. Eugene Hecht. Optics (4th Edition). Addison Wesley, 4 edition, **4** (2001) 120.
70. E. F. J. John and W. E. Galen "The ultraviolet absorption of benzotriazole", *J Am Chem Soc* **73** (1951) 4360-4362.
71. Y. C. Seow, S. P. Lim and H. P. Lee, "Microlight distribution system via optofluidic cascading prisms", *Microfluid. Nanofluid.* **11** (2011) 451-458.
72. K. Mitsui, Y. Handa, K. Kajikawa, "Optical fiber affinity biosensor based on localized surface plasmon resonance", *Appl. Phys. Lett.* **85** (2004) 4231:1-4231:3.
73. Y. C. Seow, S. P. Lim, B. C. Khoo and H. P. Lee, "An optofluidic refractive index sensor based on partial refraction", *Sens. Actuator B:Chem* (2010) doi:10.1016/j.snb.2010.03.076.
74. C. L. Song, N. T. Nguyen, A. K. Asundi and C. L. N. Low "A tunable optofluidic aperture configured by liquid core liquid cladding structure", *Optics Lett*. **34** (2009) 1767-1769.
75. Y. Yang, A. Q. Liu, L. K. Chin, X. M. Zhang, D. P. Tsai, C. L. Lin, C. Lu, G. P. Wang and N. I. Zheludev "Optofluidic waveguide as a transformation optics device for Lightwave bending and manipulation", *Nat. Commun.* **3** (2012) 651.

76. C. L. Song, N. T. Nguyen, S. H. Tan and A. K. Asundi "Modelling and optimization of micro optofluidic lenses", *Lab Chip* **9** (2009) 1178.

77. V. Mengeaud, J. Josserand and H. H. Girault "Mixing processes in a zigzag microchannel: finite element simulations and optical study", *Anal. Chem*. **74** (2002) 4279.

78. J. Seo and L. P. Lee "Disposable integrated microfluidics with self-aligned planar microlenses", *Sens. Actuators B* **99** (2004) 615.

79. J. Godin, V. Lien and Y. H. Lo "Demonstration of two-dimensional fluidic lens for integration into microfluidic flow cytometry", *Appl. Phys. Lett*. **89** (2006) 061106.

80. Z. G. Li, Y. Yang, X. M. Zhang, A. Q. Liu, J. B. Zhang, L. Cheng and Z. H. Li "Tunable visual color filter using microfluidic grating", *Biomicrofluidics* **4** (2010) 043013.

81. Y. C. Seow, S. P. Lim and H. P. Lee "Optofluidic variable-focus lenses for light Manipulation", *Lab Chip* **12** (2012) 3810-3815.

82. Morgan, J. Introduction to Geometrical and Physical Optics. New York: McGraw-Hill (1953) 57.

83. C. Monat, P. Domachuk and B. J. Eggleton "Integrated optofluidic: a new river of light", *Nat. Photonics* **1** (2007) 106.

84. H. Schmidt and A. R. Hawkins "The photonic integration of non-solid media using optofluidics", *Nat. Photonics* **5** (2011) 598.

85. W. Z. Song and J. H. Yang "Optofluidic differential spectroscopy for absorbance detection of sub-nanoliter liquid sample", *Lab Chip* **12** (2012) 1251-1254.

86. Y. Yang, A. Q. Liu, L. Lei, L. K. Chin, C. D. Ohl, Q. J. Wang and H. S. Yoon "A tunable 3D optofluidic waveguide dye laser via two centrifugal dean flow streams", *Lab Chip* **11** (2011) 3182-3187.

87. S. Xiong, A. Q. Liu, L. K. Chin and Y. Yang "An optofluidic prism tuned by two laminar flows", *Lab Chip* **11** (2011) 1864-1869.

88. L. K. Chin, A. Q. Liu, C. S. Lim, C. L. Lin, T. C. Ayi and P. H. Yap "An optofluidic volume refractometer using Fabry-Perot resonator with tunable liquid microlenses", *Biomicrofluidics* **4** (2010) 024107.

Publications

1) Y. C. Seow, S. P. Lim, B. C. Khoo and H. P. Lee, "An optofluidic refractive index sensor based on partial refraction", *Sens. Actuator B:Chem* (2010) doi:10.1016/j.snb.2010.03.076.

2) Y. C. Seow, S. P. Lim, H. P. Lee, "Tunable optofluidic switch via hydrodynamic control of laminar flow rate", *Appl.Phys. Lett.* **95** (2009) 114105.

3) Y. C. Seow, S. P. Lim and H. P. Lee, "Microlight distribution system via optofluidic cascading prisms", *Microfluid. Nanofluid.* **11** (2011) 451-458.

4) Y. C. Seow, S. P. Lim and H. P. Lee "Optofluidic variable-focus lenses for light Manipulation", *Lab Chip* **12** (2012) 3810-3815.